PHILOSOPHICAL TRANSACTIONS OF THE ROYAL SOCIETY A MATHEMATICAL, PHYSICAL & ENGINEERING SCIENCES

Defect Structure and Chemistry of (Ca$_{x}$Sr $_{1-x}$)$_{n+1}$ Ti$_{n}$O$_{3n+1}$ Layer Perovskites

Kate Hawkins and T. J. White

Phil. Trans. R. Soc. Lond. A 1991 **336**, 541-569
doi: 10.1098/rsta.1991.0099

Defect structure and chemistry of $(Ca_xSr_{1-x})_{n+1}Ti_nO_{3n+1}$ layer perovskites

By Kate Hawkins[1]† and T. J. White[2]†

[1] *Advanced Materials Program, Australian Nuclear Science and Technology Organisation, Private Mail Bag No. 1, Menai, New South Wales 2234, Australia*

[2] *National Advanced Materials Analytical Centre, School of Physics, The University of Melbourne, Parkville, Victoria 3052, Australia*

Contents

The Ruddlesden–Popper structural family is constructed from ordered intergrowths of rocksalt type (AX) layers with perovskite (ABX_3) blocks of varying widths, yielding phases with the general formula $nABX_3 \cdot AX$ where $1 < n < \infty$. In this article, the characterization of $(Ca_xSr_{1-x})_{n+1}Ti_nO_{3n+1}$ layer perovskites by powder X-ray and neutron diffraction and high resolution electron microscopy is described. These phases undergo a phase transition from tetragonal to orthorhombic symmetry at $x \approx 0.65$. Structure solutions of neutron diffraction data are presented for the end-member phases $Sr_3Ti_2O_7$ ($I4/mmm$), $Ca_3Ti_2O_7$($Ccm2_1$) and $Ca_4Ti_3O_{10}$($Pcab$). Refinement of the mixed alkaline earth preparation $(Ca_{0.85}Sr_{0.15})_4Ti_3O_{10}$ showed that Sr partitioned preferentially to the perovskite blocks rather than the rocksalt layers. Ordered and disordered intergrowths of rocksalt layers were found on the

† Present address: Electron Microscope Centre, University of Queensland, Queensland 4077, Australia.

Phil. Trans. R. Soc. Lond. A (1991) **336**, 541–569
Printed in Great Britain

$\{101\}_{orth} \equiv \{100\}_{tet}$ perovskite planes with extensive disorder most prevalent in samples annealed for short periods (less than 24 hours). Evidence is presented for the existence of V''_A and V''''_{Ti} point defects in the intermediate structures that precede the formation of ordered layer sequences. These data are discussed in terms of existing thermodynamic and structural information. For generalized Ruddlesden–Popper phases the relation between chemistry and symmetry is reviewed and factors contributing to the stability of different n-members enunciated. For completeness, the $(Ca_xSr_{1-x})_{n+1}Ti_nO_{3n+1}$ perovskites are considered as the structural prototypes of the oxide superconductors being a subset of an extended $nABX_3 \cdot mAX$ Ruddlesden–Popper family.

1. Introduction

Natural perovskite, $CaTiO_3$ is the prototype of a structural family which has the general formula ABX_3, where A and B represent larger and smaller cations respectively, and X is oxygen or halide. In addition to being chemically diverse, perovskite structures can accommodate gross stoichiometric variation by the systematic formation of several types of extended defect. This facility gives rise to polysomatism and many homologous series have been reported involving both variation in the A/B cation ratio (see, for example, Hutchison *et al.* 1977) and the cation–anion ratio (Nanot *et al.* 1976; Reller *et al.* 1984; Vallet-Regi *et al.* 1984).

The present work is concerned with perovskites which contain an excess of A atoms and conform to the general stoichiometry of $A_{n+1}B_nX_{3n+1}$. These compounds are conveniently described by the crystal chemical formula $nABX_3 \cdot AX$, $1 < n < \infty$, which emphasizes both the stoichiometric relation to the perovskite aristotype and the polysomatic interleaving of ABX_3 perovskite blocks with AX layers of the rocksalt-type structure. Figure 1 shows the relation between two perovskite structural units in the $n = 3$ member. This structural family was recognized simultaneously by Drys & Trzebiatowski (1957), Lukaszewicz (1958, 1959) and Ruddlesden & Popper (1957, 1958) who used powder X-ray diffraction (XRD) to deduce the structures of Sr_2TiO_4 ($n = 1$), $Sr_3Ti_2O_7$ ($n = 2$), and $Sr_4Ti_3O_{10}$ ($n = 3$) (table 1). All these phases are tetragonal (I4/mmm) and are based on a cubic $SrTiO_3$ perovskite subcell. Shortly afterwards, Roth (1958) reported the existence of analogous $Ca_{n+1}Ti_nO_{3n+1}$ compounds with orthorhombic $CaTiO_3$ perovskite as the basic structural unit. Subsequently, a great variety of compounds belonging to this polysomatic series have been identified. For the $n = 1$ member over 60 chemically distinct systems have been identified (at room temperature and pressure), whereas the higher members have been described less frequently: to our knowledge at least ten compounds for $n = 2$ and seven for $n = 3$. Longer period structures ($n > 4$) have not been reported as single-phase materials, although Tilley (1977) found higher members as coherent intergrowths with lower members in the SrO–TiO_2 system.

In this article, we extend the work of Tilley by describing the structures and defect chemistry of $(Ca_xSr_{1-x})_{n+1}Ti_nO_{3n+1}$ Ruddlesden–Popper phases. This system was chosen because of its importance in electronic ceramics (Han *et al.* 1985), and our interest in the interaction between subcell symmetry and extended defect formation. Our investigations proceeded in two steps. First, Rietveld analysis of powder neutron diffraction (ND) data was used to solve the structures of the

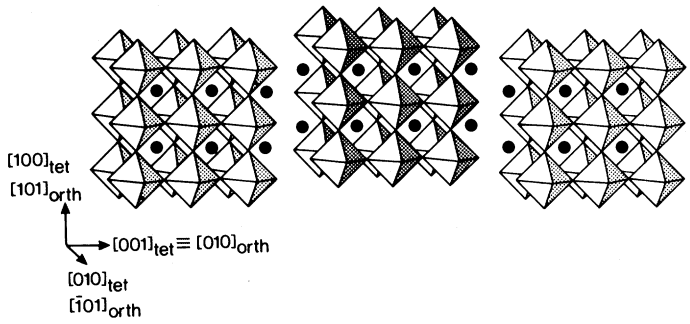

Figure 1. Schematic, perspective drawing of $3ABX_3 \cdot AX$ giving the relation between tetragonal and orthorhombic settings.

Table 1. *Symmetry of layer perovskites at room temperature and pressure*

ABX_3 phase	ABX_3 variance from cubic, S^2[a]	symmetry–unit-cell parameters (Å)			
		$n = \infty$	$n = 1$	$n = 2$	$n = 3$
$SrTiO_3$	0	Pm3m[b] $a = 3.905$	I4/mmm[c] $a = 3.88$ $c = 12.60$	I4/mmm[d] $a = 3.9026$ $c = 20.3716$	I4/mmm[c] $a = 3.90$ $c = 28.1$
$CaMnO_3$	4.2×10^{-3}	Pnma[e] $a = 5.279$ $b = 7.448$ $c = 5.264$	tet[f] $a = 3.667$ $c = 12.063$	tet[f] $a = 3.709$ $c = 19.44$	tet[f] $a = 3.724$ $c = 29.60$
$SrZrO_3$	1.4×10^{-3}	Pnma[f] $a = 5.786$ $b = 8.196$ $c = 5.814$	tet[h] $a = 4.112$ $c = 12.58$	ortho[h] $a = 5.798$ $b = 20.94$ $c = 5.808$	ortho[h] $a = 5.795$ $b = 29.34$ $c = 5.814$
$CaTiO_3$	3.3×10^{-2}	Pnma[i] $a = 5.3796$ $b = 7.6401$ $c = 5.4424$	not reported	$Ccm2_1$[d] $a = 5.4172$ $b = 19.5169$ $c = 5.4234$	Pcab[d] $a = 5.4083$ $b = 27.1432$ $c = 5.4337$

[a] Variance from cubic, $S^2 = \frac{1}{2}\sum_{i=1}^{3}(a_i - \bar{a})^2$, where a_i are the pseudocube edges.

[b] Megaw (1973). [c] Ruddlesden & Popper (1958). [d] Elcombe *et al.* (1990). [e] Poeppelmeier *et al.* (1982). [f] MacChesney *et al.* (1965). [g] Ahtee *et al.* (1976). [h] Tilloca & Perez y Jorba (1968). [i] Sasaki *et al.* (1987).

$n = 2$ and $n = 3$ calcium end members. These structures are compared with that of the $n = 2$ strontium end member, which was refined from the original structure inferred by Ruddlesden & Popper. The partitioning of calcium and strontium between the perovskite structural units and rocksalt layers was determined for $(Ca_{0.85}Sr_{0.15})_4Ti_3O_{10}$. An extended description of the refinement processes and structures are given in a companion paper (Elcombe *et al.* 1991). Secondly, drawing on these crystal structure solutions, the defect nature of calcium-rich members was studied by high-resolution electron microscopy (HREM) supported by image simulation. By using these data, we critically review the literature concerning

PHILOSOPHICAL TRANSACTIONS OF THE ROYAL SOCIETY A MATHEMATICAL, PHYSICAL & ENGINEERING SCIENCES

experimentally derived heats of formation and those calculated using an atomistic approach, and contrast our defect models with those inferred from electrical measurements.

2. Experimental methods

(a) *Materials preparation*

Polycrystalline samples were prepared by mixing appropriate quantities of analytical grade $CaCO_3$, TiO_2 and $SrCO_3$ for 5 min in a laboratory tungsten carbide ball mill. The powders was calcined at 900 °C for 1 h in air, furnace cooled, then sized to −74 μm and stored in a desiccator. They were pressed into cylindrical pellets (13 mm diameter, 2–5 mm height) as needed, using 1300 kg m^{-2} pressure for 7 min. Layered compounds with n nominally equal to ∞ (perovskite), 1, 2, 3, 5 and 10, corresponding to variable x were fabricated. The firing conditions and stoichiometries are summarized in table 2.

(b) X-*ray and neutron diffraction*

X-ray diffraction (XRD) was used for preliminary specimen characterization. Fired pellets were lightly abraded on 1200 grit silicon carbide papers then examined on a Philips PW 1050/10 diffractometer by step-scanning at 0.5°2θ min^{-1} using 0.5°2θ sampling intervals. A Co line-focus tube ($\bar{\lambda}$ = 1.790 26 Å†) was used. The angular range of 5–80°2θ was chosen as this allowed detection of low-angle supercell reflections. The results of XRD characterization are presented in table 2. For strontium-rich materials it became impossible to identify n-members due to the weak intensity of low-angle superstructure reflections. Using standard algorithms (Fischer-Cripps 1988), peak positions were determined by fitting the experimental profile to a quadratic function after smoothing over 3-interval segments. Unit cell parameters were refined by an iterative least-squares analysis of the smoothed and fitted data using FINAX (Hoverstreydt 1983) referenced to an internal Si standard. Residuals of 2–4 % were achieved.

The progression from tetragonal to orthorhombic symmetry was quantified for the $n = \infty$ member with variable x. For other n-values the correlation between symmetry and Ca:Sr ratio was established by inspection of the split 044/440 orthorhombic subcell peaks. Higher resolution XRD traces were collected for $Ca_3Ti_2O_7$ and $Ca_4Ti_3O_{10}$ in which the diffractometer was step-scanned between 5 and 120°2θ at 0.5°2θ min^{-1} using 0.05°2θ steps. To alleviate preferred orientation effects, these pellets were crushed to −74 μm and lightly pressed flat into an Al holder.

Neutron diffractometer patterns were obtained for perovskites with nominal compositions $Sr_3Ti_2O_7$, $Ca_3Ti_2O_7$, $Ca_4Ti_3O_{10}$ and $(Ca_{0.85}Sr_{0.15})_4Ti_3O_{10}$. These materials were fired for longer times than those prepared for electron microscopy to minimize disorder (table 2). The absence of polysomatic disorder was confirmed by selected area electron diffraction (SAD) and lattice imaging. Approximately 10 g of each material was crushed to −74 μm and loaded into a 1 cm diameter vanadium can. Data were collected at a wavelength of 1.893 Å over a 2θ range of −12–160° with a collection interval of 0.05°2θ. Further details of our experimental procedures are given in Elcombe *et al.* (1991).

† 1 Å = 10^{-10} m = 10^{-1} nm.

(*c*) *High-resolution electron microscopy and electron diffraction*

Specimens were prepared for electron microscopy either by crushing under ethanol to make a suspension which was dried onto holey carbon grids, or by argon ion-beam thinning with 4 keV ions at a current of 1 mA and an angle of 15°. Selected area electron diffraction, energy dispersive X-ray spectrum (EDS) analysis and routine HREM were conducted on JEM 2000FX and JEM 200CX electron microscopes operated at 200 keV. Systematic absences in SAD patterns were studied at 100 keV using a $\pm 60°$ tilt–rotate holder fitted to JEM 100CX microscope. Atomic resolution electron micrographs were obtained on a JEM 4000EX instrument operated at 400 keV and having (manufacturer specified) coefficients of spherical aberration (C_s) and chromatic aberration (C_c) of 1.0 mm and 1.7 mm respectively. The Schertzer crossover was calculated to be near to -400 Å. The objective aperture included all diffracted beams within a radius of 1.4 Å^{-1}. Thin crystals that protruded over holes in the carbon films were oriented along the $\langle 101 \rangle_{orth}$ and $\langle 100 \rangle / \langle 010 \rangle_{tet}$ poles, as these permitted direct observation of the layering sequence along the supercell direction. Through-focal series (TFS) of images were recorded with the aid of a low-light television system in defocus steps of 12 Å at magnifications of 600 000–800 000.

Experimental high-resolution images were interpreted by visual comparison with simulated images computed by multislice methods (Glaisher 1985). Initially, the association between image and structure was established for perfectly ordered sequences. For image simulation, defocus settings representing the first contrast transfer function crossover and the following contrast inversion were calculated at a beam divergence of between 1–3 mrad. Beam tilt and objective lens astigmatism were assumed to be negligible. These conditions were adequate to realize the direct structural interpretation of disordered regions.

Optical diffractograms, recorded directly from micrographs using a He–Ne laser optical bench, were used to deconvolute experimental SAD patterns. This technique was used to determine the orientation of finely textured twin domains and confirm n-values within disordered intergrowths.

High resolution imaging at 400 keV was concentrated on the calcium-rich members ($x \geqslant 0.7$) since charging of these specimens did not degrade image quality. Imaging strontium-rich material ($x \leqslant 0.3$) was less successful as specimen oscillation induced by charging was severe; the standard practice of lightly coating crystals with an evaporated carbon film failed to stabilize them. Argon ion-beam thinned specimens were useful for high-resolution imaging, although working time was shortened due to the accumulation of contaminating surface layers of amorphous hydrocarbons.

Even though the calcium-rich crystals were reasonably stable in the electron beam, *in situ* reduction occurred when observations in local areas were extended to periods of more than 15–20 min. An example of such a surface layer is shown in figure 2. By using optical diffractometry and image simulation the layer has been identified as titanium monoxide, related topotaxially to the perovskite substrate according to the orientation relation $(111)_{TiO} \parallel (111)_{orth}$. The variable contrast of the image, the distortion of the crystallographic planes, and the localized breaches of topotaxy, suggest that the TiO is probably non-stoichiometric. As the formation of TiO proceeds slowly and does not extend beyond a few monolayers we are confident that electron beam-induced decomposition will not invalidate interpretation of the images presented herein.

PHILOSOPHICAL TRANSACTIONS OF THE ROYAL SOCIETY A MATHEMATICAL, PHYSICAL & ENGINEERING SCIENCES

Table 2. *Fabrication and characterization*
(T is unreacted TiO_2.)

specimen	stoichiometry: nominal n-member	stoichiometry: x	fabrication firing conditions	characterization: XRD	characterization: SAD/HREM
EMG74A	1	0.75	1500 °C, 4.5 h, air quenched	—	$n = 3$, intergrown with $n > 3$; twinned $n = \infty$
EMG74AR	1	0.75	1500 °C, 13 h, water quenched	3	$n = 3$ intergrown with $n > 3$; twinned $n = \infty$
EMG95	2	1.00	1500 °C, 72 h; crush resize; 1500 °C, 120 h	2	perfect $n = 2$; rare isolated intergrowth $n = 3$ and $n = 4$ members
EMG81	3	0.00	1500 °C, 2 h, air quenched from 1100 °C	3[a]	—
EMG83B	3	0.50	1500 °C, 2 h, air quenched from 1100 °C	3[a]	—
EMG84B	3	0.60	1500 °C, 2 h, air quenched from 1100 °C	3[a]	—
EMG85B	3	0.75	1500 °C, 2 h, air quenched from 1100 °C	3	—
EMG86B	3	0.85	1500 °C, 2 h, air quenched from 1100 °C	3	—
EMG87B	3	1.00	1500 °C, 2 h, air quenched from 1100 °C	3, 2	$n = 2$, 3; faulted $n = 2$
EMG84C/D	3	0.60	1500 °C, 2 h; crush resize; 1500 °C, 2 h, furnace cool	3[a]	—
EMG85C/D	3	0.75	1500 °C, 2 h; crush resize; 1500 °C, 2 h, furnace cool	3	perfect $n = 3$; $n = 3$ intergrown $n = \infty$
EMG85E/F	3	0.75	1500 °C, 7.5 h, furnace cool	3	perfect $n = 3$; $n = 3$ intergrown with $n = 6$
EMG84G	3	0.60	1500 °C, 7.5 h; crush, resize; 1500 °C, 5 h; furnace cool	3	—
EMG85G	3	0.75	1500 °C, 7.5 h; crush, resize; 1500 °C, 5 h; furnace cool	3	intergrowths with $2 = n > 3$
EMG86R	3	0.85	1500 °C, 72 h; furnace cool	3	perfect $n = 3$; $n = 3$ intergrowths with $2 = n > 3$
EMG87R	3	1.00	1500 °C, 72 h; furnace cool	3	perfect $n = 2$, 3; $n = 3$; intergrown with perovskite ($n > 10$)
EMG96	3	0.85	1500 °C, 72 h; crush, resize; 1500 °C, 120 h; furnace cool	3	perfect $n = 3$; rare and isolated intergrowth with $n = 2$ and 4
EMG94	3	1.00	1500 °C, 72 h; crush, resize; 1500 °C, 120 h; furnace cool	3, minor 2	perfect $n = 3$
EMG77A	5	0.75	1500 °C, 4.5 h, air quenched	—	—
EMG76AR	5	1.00	1500 °C, 4.5 h, air quenched; 1500 °C, 8 h, water quenched	—	$n = 3$ intergrown with $n > 10$; perfect $n = 3$, ∞; twin mosaics
EMG31	10	0.18	1500 °C, 24 h, furnace cool	∞, T	$n = 2$, 3, ∞; $n = 3$ intergrown with $n > 10$; unreacted material
EMG34	10	0.27	1500 °C, 24 h, furnace cool	∞, T	—
EMG30	10	0.45	1500 °C, 24 h, furnace cool	∞, T	$n = 3$, ∞; $n = 3$ intergrown with $n = 4$, 5, 6; twin mosaics
EMG33	10	0.55	1500 °C, 24 h, furnace cool	∞, minor $n = 2$, 3	$n = 2$, 3, ∞; $n = 3$ intergrown with $n = 4$, 5, 6, 7, 9, > 10; twin mosaics

PHILOSOPHICAL TRANSACTIONS OF THE ROYAL SOCIETY A MATHEMATICAL, PHYSICAL & ENGINEERING SCIENCES

Table 2 (*cont.*)

specimen	stoichiometry: nominal n-member	stoichiometry: x	fabrication firing conditions	characterization: XRD	characterization: SAD/HREM
EMG29		0.72		∞, minor $n = 2, 3$	$n = 2, 3, 4, \infty$; $n = 3$ intergrown with $n = 2, 4, 5, 6, 7, > 10$
EMG32		0.82		∞, minor $n = 2, 3$	$n = 3, \infty$; $n = 3$ intergrown with $n = 5, > 10$
EMG17R1		0.00		∞	$n = \infty$; $n = 3$ intergrown with $n = 2, 4, 6, 7, 8, 10$ and significant amounts of $n = 5$ and $n > 10$; twin mosaics
EMG16R1		0.10		∞	$n = \infty$; $n = 3$ intergrown with $n = 4, 5, 6, > 10$; twin mosaics
EMG15R1		0.20		∞	$n = \infty$; disordered $n = 2$
EMG14R1		0.30		∞	—
EMG13R1		0.40		∞	$n = \infty$; $n = 2$ intergrown with $n = 3, 5$
EMG12R1	∞	0.50	1500 °C, 24 h, furnace cool	∞	$n = 3, \infty$; $n = 3$ intergrown with $n = 4, 5, 7$
EMG11R1		0.60		∞	$n = \infty$ with isolated $n = 3$ layers; $n = 3$ intergrown with $n = 4, 5, 6, 7, 9, > 10$
EMG10R1		0.70		∞	$n = 3, \infty$; $n = 4$ intergrown with $n = 7$; twin mosaics
EMG9R1		0.80		∞	$n = \infty$; $n = 4$ intergrown with $n = 4, 6, 8$
EMG8R1		0.90		∞	$n = 4, 5, \infty$; $n = 3$ intergrown with $n = 4, 9$
EMG7R1		1.00		∞	$n = 3, \infty$; $n = 3$ intergrown with $n > 10$; twin mosaics
EMG12R2		0.50		∞	twinned $n = \infty$
EMG9R2	∞	0.80	1500 °C, 96 h, furnace cool	∞	twinned $n = \infty$; minor unreacted material
EMG8R2		0.90		∞	twinned $n = \infty$
EMG10A	∞	0.70	1475 °C, 72 h, furnace cool	∞	twinned $n = \infty$; $n = 3$ intergrown with $n > 10$
EMG2	∞	0.80	1480 °C, 144 h, furnace cool	∞	$n = \infty$; heavily disordered $n = 3$, 4 intergrown with $2 < n < \infty$; twin mosaics

[a] $n = 3$ and $n = \infty$ could not always be distinguished unambiguously in Sr-rich materials.

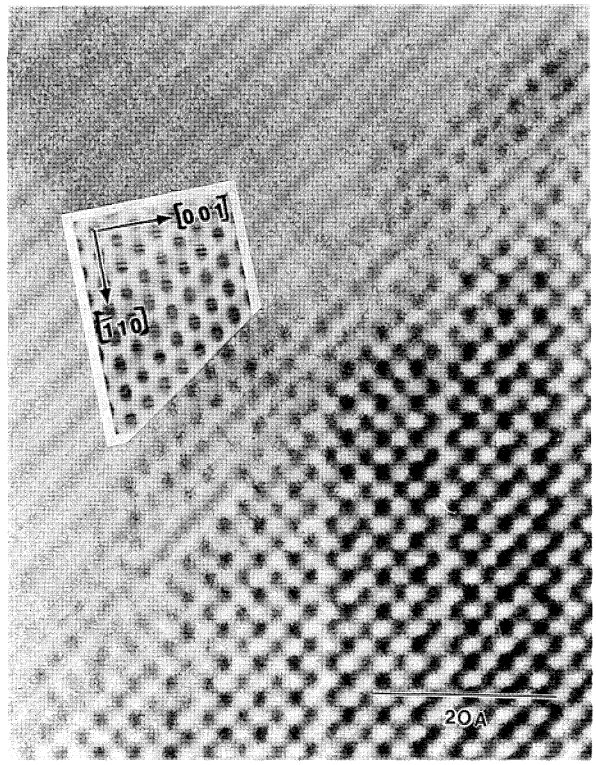

Figure 2. [110] TiO_x surface layer arising from electron beam-induced reduction of $3CaTiO_3 \cdot CaO$. (Calculation parameters: $T = 18$ Å; $\Delta f = -375$ Å.)

3. Correlations between chemistry and crystallography

(a) *Orthorhombic–tetragonal transition*

The complete solid solution between $SrTiO_3$ and $CaTiO_3$ perovskites ($n = \infty$) has been known for some time (Durst *et al.* 1950; Kwestroo & Paping 1959). By using the Nelson–Riley function and a pseudomonoclinic setting McQuarrie (1955) extrapolated back from $CaTiO_3$ ($\beta = 90°40'$) to a tetragonal intermediate ($\beta = 90°$) at $x = 0.45$, then to a cubic structure at $x = 0.15$. To confirm this result we examined a number of $(Ca_xSr_{1-x})TiO_3$ compositions by XRD and SAD. Our results are summarized in figure 3*a*. Within the limits of diffractometer resolution perovskite switched from tetragonal to orthorhombic symmetry at approximately $(Ca_{0.65}Sr_{0.35})TiO_3$. For $n = \infty$ SAD was not a satisfactory means of establishing symmetry due to double diffraction.

The transition from orthorhombic to tetragonal symmetry for $n = 3$ members in passing from $Ca_4Ti_3O_{10}$ to $Sr_4Ti_3O_{10}$ was also studied. The pair of lines chosen was the 440/044 orthorhombic subcell pair lying close to $2\theta = 87°$, since these are the highest-angle (pseudo-tetragonal) pair of reasonable intensity for which there is no interlocation of other lines. By using this technique, the symmetry transition was found at $x = 0.65$ (figure 3*b*), although electron diffraction indicates that orthorhombic symmetry persists to higher Ca/Sr ratios ($x = 0.70$). This discrepancy is to be expected as the observation of 440/044 splitting is dependent upon

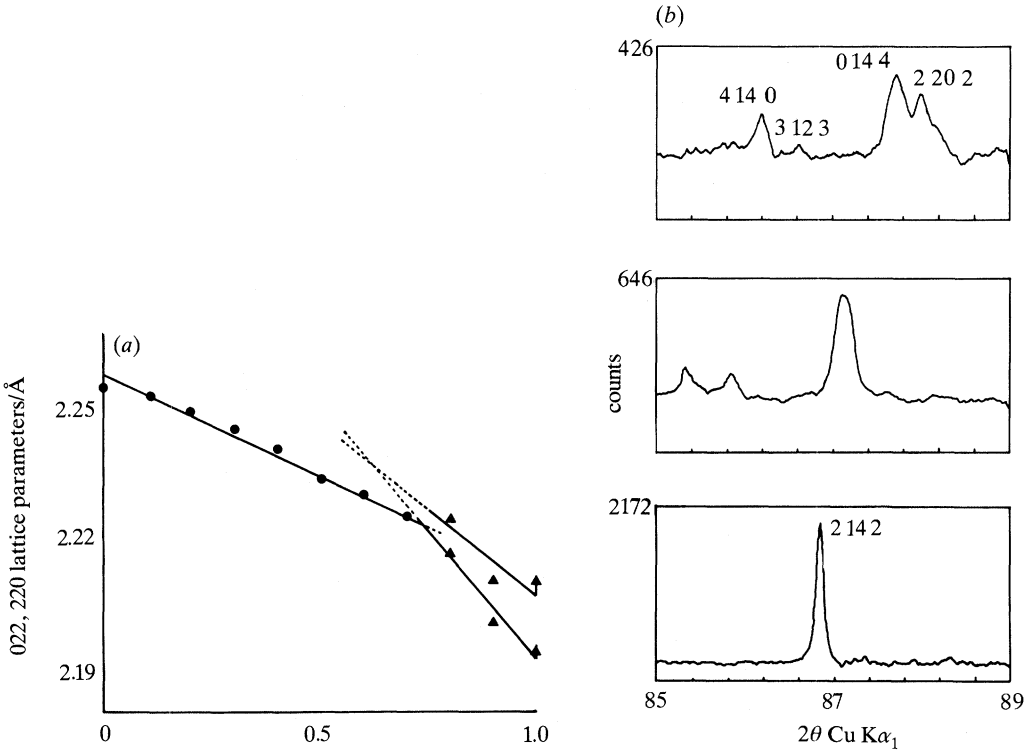

Figure 3. (*a*) Relation between symmetry and calcium content for perovskite, $n = \infty$. ●, tetragonal; ▲, orthorhombic. (*b*) Convergence of (0.14.4) and (2.20.2) orthorhombic reflections towards the tetragonal (2.14.2) reflection in the $n = 3$ polytype. From top to bottom the compositions are $Ca_4Ti_3O_{10}$, $Ca_3SrTi_3O_{10}$ and $Ca_2Sr_2Ti_3O_{10}$.

diffractometer resolution and will fail to distinguish a reduction in symmetry when the difference between a and c is slight. Therefore, the symmetry transitions in both perovskite ($n = \infty$) and its layered analogue ($n = 3$) occur at approximately the same composition.

(*b*) *Crystallography of calcium and strontium end members*

Our studies by powder XRD and Rietveld analysis of neutron diffraction data have confirmed I4/mmm as the space group for $Sr_3Ti_2O_7$ and arrived at lattice parameters and atomic coordinates in general agreement with Ruddlesden & Popper (1958) (table 3).

Tilloca & Perez y Jorba (1964) surmised that the symmetry of Ca end-member layer perovskites would be orthorhombic since the $CaTiO_3$ subcell possessed this symmetry. In orthorhombic structures b is fixed as the long axis, and a and c are parallel to the two-fold axes of the TiO_6 octahedra; this is consistent with the *Pnma* setting of $CaTiO_3$ (Kay & Bailey 1957). The orthorhombic unit cell is related to the tetragonal cell as follows:

$$\begin{bmatrix} a \\ b \\ c \end{bmatrix}_{\text{orth}} = \begin{bmatrix} 1 & 0 & 1 \\ 0 & 1 & 0 \\ -1 & 0 & 1 \end{bmatrix} \begin{bmatrix} a \\ c \\ b \end{bmatrix}_{\text{tet}}.$$

Table 3. *Unit cell contents of* $Sr_3Ti_2O_7$
(S.G. I4/mmm (no. 139), $a = 3.9026$ (1) Å, $c = 20.3716$ Å.)

atom	x	y	z
Sr(1)	$\frac{1}{2}$	$\frac{1}{2}$	0
Sr(2)	$\frac{1}{2}$	$\frac{1}{2}$	0.1842 (1)
Ti	0	0	0.0964 (3)
O(1)	0	0	0
O(2)	0	0	0.1934 (2)
O(3)	0	$\frac{1}{2}$	0.0961 (1)

Table 4. *Unit cell contents of* $Ca_3Ti_2O_7$
(S.G. $Ccm2_1$ (no. 36), $a = 5.4172$ (1) Å, $b = 19.5169$ (4) Å, $c = 5.4234$ (1) Å.)

atom	x	y	z
Ca(1)	0.2517 (9)	0	0.0290 (12)
Ca(2)	0.7410 (5)	0.1876 (2)	0.4747 (8)
Ti	0.2491 (9)	0.0989 (2)	$\frac{1}{2}$
O(1)	0.8124 (6)	0	−0.0132 (3)
O(2)	0.6958 (5)	0.1972 (1)	0.0132 (3)
O(3)	0.5378 (2)	0.0860 (1)	0.2883 (2)
O(4)	0.0378 (2)	0.1099 (1)	0.2117 (2)

Table 5. *Unit cell contents of* $Ca_4Ti_3O_{10}$
(S.G. Pcab (no. 61), $a = 5.4083$ (1) Å, $b = 27.1432$ (4) Å, $c = 5.4337$ (1) Å.)

atom	x	y	z
Ca(1)	0.5038 (8)	0.0693 (3)	0.4665 (9)
Ca(2)	0.9921 (5)	0.2053 (2)	0.0238 (12)
Ti(1)	0	0	$\frac{1}{2}$
Ti(2)	0.4973 (13)	0.1426 (2)	0
O(1)	0.4332 (5)	0.0708 (2)	0.0142 (3)
O(2)	0.5548 (8)	0.2118 (2)	0.9858 (3)
O(3)	0.7125 (8)	0.1321 (1)	0.7115 (2)
O(4)	0.2875 (7)	0.1499 (1)	0.2885 (2)
O(5)	0.2099 (7)	0.9900 (2)	0.7885 (2)

In this study and earlier investigations (Coughanour *et al.* 1954; Roth 1958; Kwestroo & Paping 1959; Tilloca & Perez y Jorba 1964) the orthorhombic nature of the $Ca_4Ti_3O_{10}$ and $Ca_3Ti_2O_7$ phases were confirmed by XRD. However, the space groups were not determined conclusively by XRD, as the extinction of (hkl), ($0kl$), ($h0l$) and ($0kl$) reflections could not be unambiguously determined. Further, our SAD pattern tilt sequences did not provide unequivocal limiting conditions for ($h00$), ($0k0$) and ($00l$) with $h, k, l = 2n$.

Therefore, it was necessary to adopt a fundamental approach for the development of model structures for Rietveld refinement, in which the symmetry operators and atom positions for $CaTiO_3$, whose structure is well known (Kay & Bailey 1957; Koopmans *et al.* 1983; Sasaki *et al.* 1987), were used to construct the layer perovskites. In this way the space groups were deduced to be $Ccm2_1$ (no. 36) for $Ca_3Ti_2O_7$ and Pcab (no. 61) for $Ca_4Ti_3O_{10}$. Starting with these models full matrix least squares analysis of all atom positions and isotropic temperature factors for the

PHILOSOPHICAL TRANSACTIONS OF THE ROYAL SOCIETY A MATHEMATICAL, PHYSICAL & ENGINEERING SCIENCES

Table 6. *Calculated and observed X-ray diffraction patterns of* $Ca_3Ti_2O_7$, *using* CoKα *radiation, using lattice parameters obtained from Rietveld refinement of neutron data. Patterns are compared with d-spacings calculated from the results of previous workers, using their lattice parameters.*

hkl orthorhombic indexing			this work					Coughanour *et al.* (1954)		Roth (1958)		Kwestroo & Paping (1959)		Tilloca & Perez y Jorba (1964)
			d_{calc}	$I/I_{0,\,calc}$	$2\theta_{obs}$	d_{obs}	$I/I_{0,obs}$	d_{exp}	I/I_0	d_{exp}	I/I_0	d_{exp}	I/I_0	d_{exp}
0	2	0	9.759	15	10.519	9.765	29	9.7	29	9.73	100	9.81	14	9.752
1	1	0	5.220	<1										
0	4	0	4.879	16	21.185	4.870	53	4.9	53	4.873	100	4.88	18	4.870
1	3	0	4.163	<1										
1	1	1	3.761	7	27.548	3.760	6	3.76	1	3.762	8	3.76	6	3.763
1	3	1	3.302	3	31.466	3.301	3	3.30	<1	3.302	3	3.31	2	3.304
0	6	0	3.253	0										
1	5	0	3.167	<1										
1	5	1	2.735	100	38.151	2.739	97	2.73	23	2.733	100	2.73	100	2.733
								2.73	12					
0	0	2	2.712	38	38.517	2.714	28	2.71	10					2.710
2	0	0	2.709	36						2.708	66	2.70	81	
0	2	2	2.613	1	39.989	2.618	3	2.61	1	—				—
2	2	0	2.610	<1								2.61	2	
7	1	0	2.479	3	42.288	2.482	3	2.48	1	2.478[a]	7	—		2.479[a]
0	8	0	2.440	<1	43.016	2.442	2	2.44	1	2.439	5	—		2.440
2	0	1	2.423	1	43.295	2.427	2	2.42	1	—		—		—
1	1	2	2.406	1	43.647	2.408	1	2.40	<1	—		—		—
0	4	2	2.370	1	44.375	2.370	2	2.37	<1	—				—
2	4	0	2.368	1								2.36	3	
2	2	1	2.352	1	44.795	2.349	3	2.35	<1	—				—
1	3	2	2.272	2	46.394	2.730	2	2.27	<1	—		—		—
1	7	1	2.255	6	46.802	2.254	7	2.25	2	2.255	11	2.25	6	2.254
2	4	1	2.170	1				2.25	1					
0	6	2	2.083	6	50.941	2.082	10	2.08	4	2.081	23	2.08	16	2.083
2	6	0	2.082	5										
1	5	2	2.060	1	51.550	2.059	2	2.06	<1	—		—		—
1	9	0	2.013	1	52.837	2.012	1	2.01	1	—		—		—
0	10	0	1.952	25	54.640	1.950	100	1.95	100	1.9505	100	1.947	35	1.952
6	2	1	1.943	<1										
2	0	2	1.916	51	55.743	1.915	30	1.92	4	1.9159	27	1.911	49	1.916
1	9	1	1.887	7	56.658	1.886	9	1.89	2	1.8871	14	1.883	8	1.888
2	2	2	1.881	2										
1	7	2	1.823	<1										
0	8	2	1.814	2	59.171	1.813	4	1.81	1	—				—
2	8	0	1.813	1								1.818	2	
1	3	0	1.798	0										
2	4	2	1.784	3	60.279	1.783	2	1.78	1	1.7836	6	1.778	2	1.783
3	3	0	1.740	1		—		1.74	<1	1.7363[a]	3	—		1.737
8	2	1	1.719	<1										
1	1	3	1.708	2	63.253	1.707	1	1.71	<1	1.7080	3	—		1.708
3	1	1	1.707	1										
1	11	0	1.686	<1	—			—		—				
1	3	3	1.658	3	65.345	1.658	2	1.66	1					1.659
3	3	1	1.657	1	65.476	1.655	1			1.6581	4	1.654	3	
2	6	2	1.651	<1										
5	3	0	1.639	<1										
0	12	0	1.624	1	66.761	1.627	6	1.63	6	1.6258	37	1.623	1	1.626
1	9	2	1.617	<1										
1	11	1	1.610	<1										
0	10	2	1.584	11										
2	10	0	1.584	10						1.5831	38	1.580	21	
1	5	3	1.570	16	69.588	1.569	18	1.57	4	1.5690	27	1.565	40	1.569
3	5	1	1.569	22										
2	10	1	1.520	<1										

PHILOSOPHICAL TRANSACTIONS OF THE ROYAL SOCIETY A MATHEMATICAL, PHYSICAL & ENGINEERING SCIENCES

Table 6 (*cont.*)

hkl orthorhombic indexing			this work					Coughanour *et al.* (1954)		Roth (1958)		Kwestroo & Paping (1959)		Tilloca & Perez y Jorba (1964)
			d_{calc}	$I/I_{0,calc}$	$2\theta_{obs}$	d_{obs}	$I/I_{0,obs}$	d_{exp}	I/I_0	d_{exp}	I/I_0	d_{exp}	I/I_0	d_{exp}
3	7	0	1.516	<1										
2	8	2	1.507	<1										
2	0	3	1.504	<1										
3	1	2	1.499	<1										
2	2	3	1.486	<1										
3	3	2	1.465	<1										
1	7	3	1.461	2	75.333	1.465	1	1.46	1					
3	7	1	1.460	1	75.532	1.462	1			1.4598	4	1.457	1	1.450

[a] Reflection recorded by previous authors, but not indexed.

Table 7. *Calculated and observed X-ray diffraction patterns of* $Ca_4Ti_3O_{10}$, *using* CoKα *radiation, using lattice parameters obtained from Rietveld refinement of neutron data. Patterns are compared with d-spacings calculated from the results of previous workers, which were collected using* CuKα *radiation*

hkl orthorhombic indexing			this work					Roth (1958)		Tilloca & Perez y Jorba (1964)
			d_{calc}/Å	$I/I_{0,calc}$	$2\theta_{obs}$	d_{obs}/Å	$I/I_{o,obs}$	d_{exp}/Å	$I/I_{0,exp}$	d_{exp}/Å
0	2	0	13.571	10	7.610	13.487	17	13.5	6	13.545
0	4	0	6.786	5	15.198	6.769	19	6.78	7	6.783
1	2	0	5.024	<1						
0	6	0	4.524	12	22.869	4.515	48	4.525	11	4.525
1	4	0	4.229	<1						
1	1	1	3.795	8	27.551	3.759	2	3.795	9	3.795
1	2	1	3.689	<1						
1	3	1	3.529	<1						
1	6	0	3.470	<1						
0	8	0	3.393	<1						
1	4	1	3.337	2	31.142	3.335	3	3.337[a]	5	3.338
1	5	1	3.131	<1						
1	6	1	2.924	<1						
1	8	0	2.874	<1						
1	7	1	2.726	100	38.432	2.720	100	2.725	100	2.725
0	0	2	2.717	35				2.718	100	2.720
0	10	0	2.714	0						2.706
2	0	0	2.704	32				2.706	46	
0	1	2	2.703	<1						
0	2	2	2.664	<1						
2	2	0	2.652	<1						
0	3	2	2.602	<1						
1	8	1	2.541	<1						
0	4	2	2.522	<1	41.791	2.509	1			
2	4	0	2.512	<1						
0	5	2	2.430	<1						
1	10	0	2.426	3	43.414	2.420	5	2.422[a]	8	2.422[b]
2	0	1	2.426	1						
1	1	2	2.418	1						
2	1	2	2.390	<1						
2	2	1	2.383	<1						

PHILOSOPHICAL TRANSACTIONS OF THE ROYAL SOCIETY A MATHEMATICAL, PHYSICAL & ENGINEERING SCIENCES

Table 7 (*cont.*)

hkl orthorhombic indexing			this work					Roth (1958)		Tilloca & Perez y Jorba (1964)
			d_{calc}/Å	$I/I_{0,calc}$	$2\theta_{obs}$	d_{obs}/Å	$I/I_{o,obs}$	d_{exp}/Å	$I/I_{0,exp}$	d_{exp}/Å
1	9	1	2.370	2	44.453	2.366	2	2.367	4	2.369
1	3	2	2.345	<1						
2	3	1	2.339	2						
0	6	2	2.329	1	45.260	2.326	2			
2	6	0	2.321	1						
1	4	2	2.286	2	46.175	2.283	2	2.283[a]	3	2.284
2	4	1	2.280	<1						
0	12	0	2.262	<1	46.851	2.252	1			
0	7	2	2.225	0						
1	5	2	2.216	<1						
1	10	1	2.215	1	47.758	2.211	1	2.212[a]	4	2.213[b]
5	2	1	2.211	<1						
1	6	2	2.139	<1						
2	6	1	2.134	1						
0	8	2	2.121	5	49.985	2.119	4			
2	8	0	2.115	5				2.116	10	2.116
1	12	0	2.087	1						
1	11	1	2.075	2	51.188	2.072	2	2.075	3	2.076
1	7	2	2.058	1						
2	7	1	2.054	0						
0	9	2	2.019	<1						
1	8	2	1.974	<1						
2	8	1	1.971	<1						
0	14	0	1.939	24	55.061	1.937	35	1.939	33	1.939
0	10	2	1.920	<1						
2	0	2	1.917	49	55.749	1.915	40	1.915	65	1.914[b]
2	10	0	1.916	<1						
2	1	2	1.912	<1						
2	2	2	1.898	<1						
1	9	2	1.891	<1	56.662	1.886	1			
2	9	1	1.888	<1						
2	3	2	1.875	1	57.076	1.874	1	1.874[a]	3	1.875
2	4	2	1.844	<1	58.135	1.842	1			
1	13	1	1.834	4	58.473α_1	1.831	6	1.832	7	1.833
0	11	2	1.827	1						
1	14	0	1.825	<1						
1	10	2	1.810	<1						
2	5	2	1.807	<1						
2	10	1	1.807	<1						
3	2	0	1.787	<1						
2	6	2	1.765	3	60.986α_1	1.762	2	1.764	6	1.765
3	4	0	1.742	1						
0	12	2	1.738	1	62.003$\bar{\alpha}$	1.738	1			
2	12	0	1.735	<1						
1	11	2	1.731	<1						
1	14	1	1.730	<1						
2	11	1	1.728	<1						
2	7	2	1.718	<1						
1	1	3	1.714	2	62.971α_1	1.713	2	1.713[b]	4	1.713
3	1	1	1.708	<1	63.420α_1	1.702	1			
1	2	3	1.704	<1						

PHILOSOPHICAL TRANSACTIONS OF THE ROYAL SOCIETY A MATHEMATICAL, PHYSICAL & ENGINEERING SCIENCES

Table 7 (*cont.*)

hkl orthorhombic indexing			this work					Roth (1958)		Tilloca & Perez y Jorba (1964)
			d_{calc}/Å	$I/I_{0,calc}$	$2\theta_{obs}$	d_{obs}/Å	$I/I_{o,obs}$	d_{exp}/Å	$I/I_{0,exp}$	d_{exp}/Å
3	2	1	1.698	<1						
0	16	0	1.696	1	63.760$\bar{\alpha}$	1.695	1			
1	3	3	1.687	<1						
3	3	1	1.681	<1						
3	6	0	1.675	<1						
2	8	2	1.669	<1	65.119$\bar{\alpha}$	1.663	1	1.664	5	1.665
1	4	3	1.665	3						
3	4	1	1.659	1						
0	13	2	1.656	<1						
1	12	2	1.655	<1						
2	12	1	1.653	0						
1	5	3	1.637	<1						
1	15	1	1.636	<1						
3	5	1	1.632	<1						
1	16	0	1.619	<1						
2	9	2	1.618	<1						
1	6	3	1.606	<1						
3	6	1	1.600	<1						
3	8	0	1.592	<1						
1	13	2	1.583	<1						
2	13	1	1.581	<1						
0	14	2	1.578	11	69.256α_1	1.574	16			
2	14	0	1.576	10	α_1			1.576	15	1.577
0	14	2			α_2					
2	14	0			69.527α_2	1.569	19			
1	7	3	1.570	16	α_1					
2	10	2	1.566	<1				1.565	40	1.565
1	7	3			69.726α_2	1.566	18			
3	7	1	1.565	22	α_1					
3	7	1			69.922α_2	1.565	7			
2	14	2	1.363	20	81.803α_1	1.366	16			
2	14	2			82.131α_2	1.363	9	1.362	21	1.362
0	0	4	1.358	5	α_1					
0	0	4			82.357α_2	1.361	3			
4	0	0	1.352	5				1.351	9	1.351
1	21	1	1.225	5	93.995α_1	1.223	13	1.224[a]	4	
					94.252α_2	1.223	8			

[a] Reflection recorded by previous authors, but not indexed.
[b] Indexing scheme by previous authors not in agreement with present work.

$n = 2$ and $n = 3$ calcium end members converged to residuals of $R_B = 1.37\,\%$ and $R_B = 1.53\,\%$ respectively. A summary of space group and unit cell data are given in tables 4 and 5.

Atom positions from these refinements were used to simulate XRD patterns for comparison with our own data and to permit re-indexing of patterns obtained by previous workers (tables 6 and 7). The data are truncated at the position where α_1/α_2 splitting makes the indexing of weak reflections ambiguous; a complete listing is available on request. For our traces of $Ca_3Ti_2O_7$ and $Ca_4Ti_3O_{10}$ there is generally good

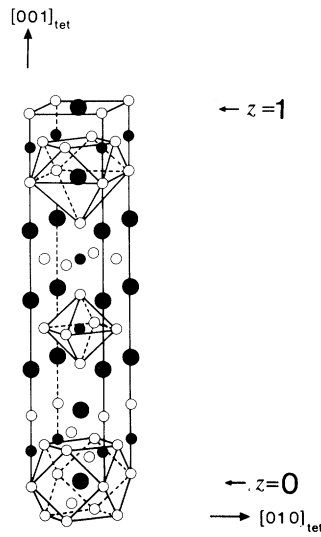

Figure 4. AO_{12}, AO_9 and BO_6 polyhedra in a tetragonal $n = 2$ polytype.

agreement between the calculated and experimental intensities. The exceptions are (0k0) reflections, which have higher than calculated intensities due to preferential cleavage on these planes. Similar enhancement of (0k0) reflections was also observed during powder neutron diffraction (Elcombe *et al.* 1991).

(*c*) *Partitioning of calcium and strontium*

Partitioning of Ca and Sr between different A sites may be expected as the covalent radius of Sr^{XII} (1.58 Å) is significantly greater than that of Ca^{XII} (1.48 Å) (Shannon 1976). There are two types of A-cation site in layered perovskites. Within the perovskite blocks is found a twelve coordinate distorted cuboctahedron. Between the blocks is a nine coordinate face capped square antiprism (figure 4).

Polyhedral volumes of the A-site polyhedra and TiO_6 octahedra were calculated using VOLCAL (Hazen & Finger 1982). The algorithm used is based on Euler's method of triangle projection (Swanson & Peterson 1980), so care was required to ensure that all exterior faces of the polyhedra were triangular. In regular cuboctahedra (as found in Sr end members) there are six rhombic faces, while in the distorted cuboctahedra of the Ca end members there are two rhombic faces. For these faces the fractional coordinates of selected atoms were minimally altered (± 0.0001) to provide convex, triangular faces consistent with the volume calculation method. The results of these calculations are summarized in table 8. The TiO_6 octahedral volumes are essentially invariant for all n-values, while the 12 coordinate A sites are 4–8 Å^3 larger than the nine coordinate sites. Therefore, it might be expected that Sr would preferentially enter the 12 coordinate A-site. This hypothesis was confirmed by refining the structure of an $n = 3$ perovskite of nominal composition $(Ca_{0.85}Sr_{0.15})_4Ti_3O_{10}$ (Elcombe *et al.* 1991). The composition was found to be $(Ca_{0.90}Sr_{0.10})Ti_3O_{10}$, with negligible partitioning of Sr into the rocksalt layers. Some $n = 2$ perovskite was also present in the sample accounting for 3% by volume, however, its Ca/Sr partitioning could not be determined as its concentration was too low. Mass balance considerations suggest it should have a composition which is relatively

Table 8. *Polyhedral volumes* (Å^3)

site	$SrO–TiO_2$ $n=1$	$n=2$	$n=3$	$n=\infty$	$CaO–TiO_2$ $n=2$	$n=3$	$n=\infty$	$(Ca,Sr)O–TiO_2$ $n=3$
AO_{12}	—	49.52	48.19	49.63	46.26	46.59	45.96	47.44
AO_9	42.70	42.80	44.13	—	38.63	38.69	—	39.04
$Ti(1)O_6$	9.63	10.00	9.69	9.93	9.92	9.62	9.96	9.78
$Ti(2)O_6$	—	—	9.69	—	—	9.61	—	9.59
ref.	(*a*)	(*b*)	(*c*)	(*d*)	(*b*)	(*b*)	(*e*)	(*b*)

(*a*) Lukaszewicz (1959), (*b*) Elcombe *et al.* (1991), (*c*) Ruddlesden & Popper (1958), (*d*) Megaw (1973), (*e*) Sasaki *et al.* (1987).

richer in Sr than the $n = 3$ phase, in agreement with the observation that Sr titanates, but not the Ca analogues, favour lower n-members (see §4*b*). There is no evidence for altervalent substitution of titanium by calcium or strontium.

4. Layer and domain structures

(*a*) *Ordered polytypes*

The structure images of ordered polytypes were directly interpretable in the $\langle 101\rangle_{orth} = \langle 100\rangle_{tet}$ zones in which the crystals are viewed along the pseudofour-fold axis of the octahedra. To examine the sensitivity of HR micrographs to changes in symmetry effected by oxygen displacement, images for the $n = 3$ member were simulated for $Ca_4Ti_3O_{10}$ by multislice calculation. The orthorhombic cell derived from neutron diffraction, and the equivalent idealized tetragonal cell were used. Comparison of the simulated images illustrates that close to Scherzer defocus neither small deviations in symmetry, nor isomorphic substitution of strontium by calcium are detectable. Therefore, to simplify our calculations, unit cells were adopted having lattice parameters of the orthorhombic cell, but the undistorted and untilted octahedra of the tetragonal cell.

$[101]_{orth}$ HR images of an $n = 3$ polytype in a compound of bulk stoichiometry $(Ca_{0.8}Sr_{0.2})TiO_3$ ($n = \infty$) are shown in figure 5. Simulated images constructed from 169 diffracted beams, are included for comparison. The TFS indicated a high-contrast image at $\Delta f = -350$ Å to -400 Å, with optimum matches at -350 Å to -375 Å and a beam divergence of 3 mrad. A contrast inversion was observed in the focal range -600 Å to -650 Å, with optimum matches achieved at -600 Å and -625 Å, and a divergence of 1 mrad. The variation in beam divergence between TFS images is due to fine adjustment of the condenser focus during experimental imaging, to compensate for diminution of image brightness arising from illumination drift.

High resolution images were also collected from the $\langle 100\rangle/\langle 001\rangle_{orth}$ zones, viewing approximately along the two-fold axis of the octahedra. Although these orientations did not yield the readily interpretable images of the $[101]_{orth}$ zone, they were nevertheless useful for determining n-value distributions and order–disorder phenomena. An experimental and simulated image for an ordered $n = 2$ crystal in a preparation of nominal composition $Ca_4Ti_3O_{10}$ ($n = 3$) is shown in figure 6.

PHILOSOPHICAL TRANSACTIONS OF THE ROYAL SOCIETY A MATHEMATICAL, PHYSICAL & ENGINEERING SCIENCES

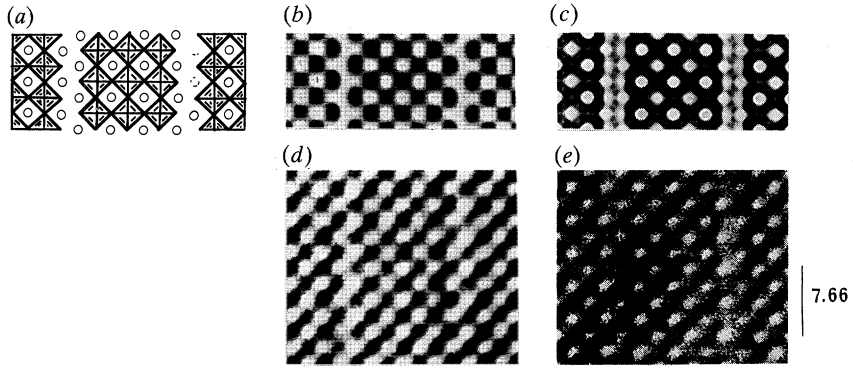

Figure 5. $[101]_{orth}$ schematic drawing (*a*) together with the simulated (*b*, *c*) and experimental (*d*, *e*) images from $Ca_4Ti_3O_{10}$. (Calculation parameters: $T = 24$ Å; $\Delta f = -375$ Å, -600 Å.) This image and subsequent high-resolution micrographs were collected using the JEM 4000EX microscope.

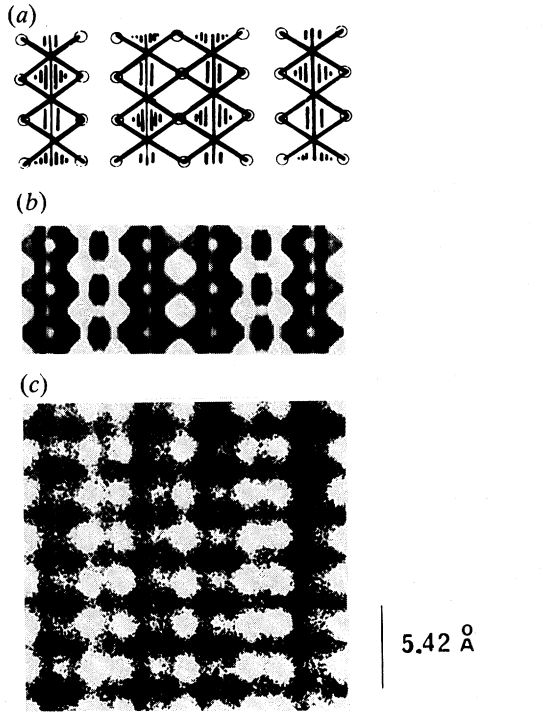

Figure 6. $[100]_{orth}$ schematic drawing (*a*) together with the simulated (*b*) and experimental (*c*) images from $Ca_3Ti_2O_7$. (Calculation parameters: $T = 50$ Å; $\Delta f = -625$ Å.)

(*b*) *Disordered polytypes*

Polysynthetic intergrowth of *n*-members was found in all preparations. Extensively disordered regions were common in materials annealed for short periods, but were observed infrequently after long-term firing (table 2). In the latter instance, disorder consisted of small isolated *n*-member anomalies in otherwise perfectly ordered structure. Quench rate had no detectable effect on disorder. No significant

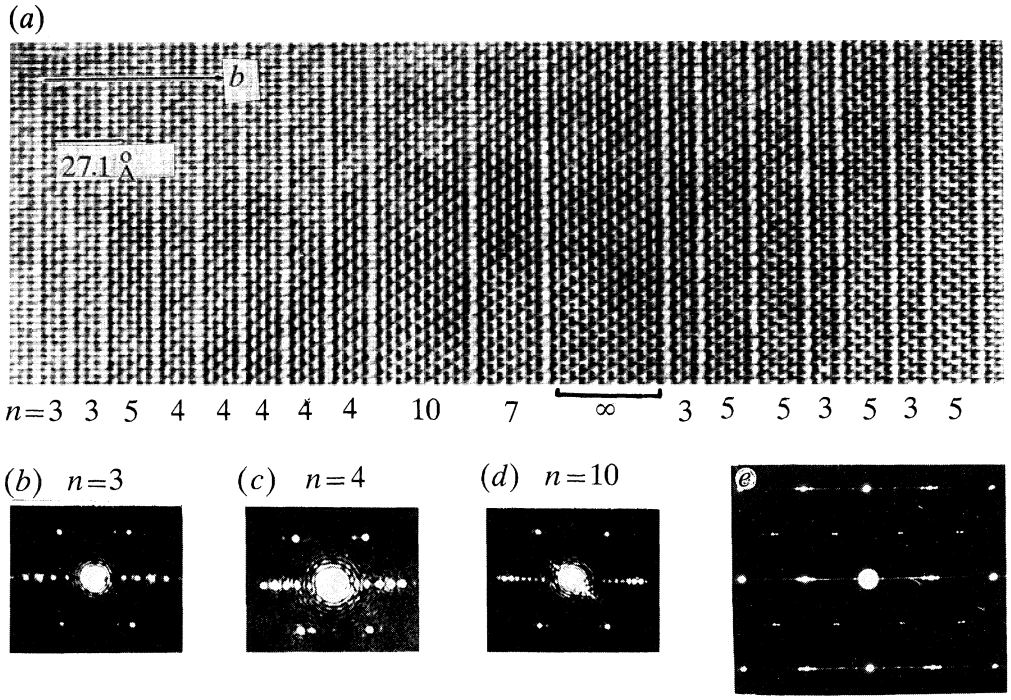

Figure 7. (*a*) $[100]_{orth}$ disordered intergrowth of polysomatic members. The fragment was from a compound of bulk stoichiometry of $Ca_4Ti_3O_{10}$ ($n = 3$) but represents a local average stoichiometry of $Ca_{5.53}Ti_{4.53}O_{14.69}$ ($n = 4.53$). The n-values were confirmed by optical diffractometry (*b–d*) which are components of the SAD pattern (*e*).

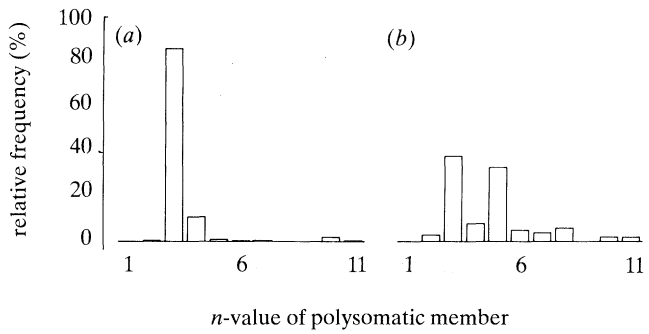

Figure 8. Frequency of occurrence histogram for (*a*) orthorhombic ($x > 0.70$) and (*b*) tetragonal ($x = 0$) n-members.

ordering of n-members to yield long-range superstructures was observed. Randomly disordered regions were common: such a crystal fragment is shown in figure 7.

The frequency of occurrence of various n-members as a function of fabrication conditions and Ca/Sr ratio was investigated. Data were collected from approximately 50 fields, equally covering all preparations, by counting lattice fringes directly from the high-resolution micrographs. (Regions of crystal representing a polysomatic member where $n > 10$ were not counted as an n-member, but were treated as an intergrowth of unfaulted perovskite structure. The value of $n > 10$ was arbitrarily

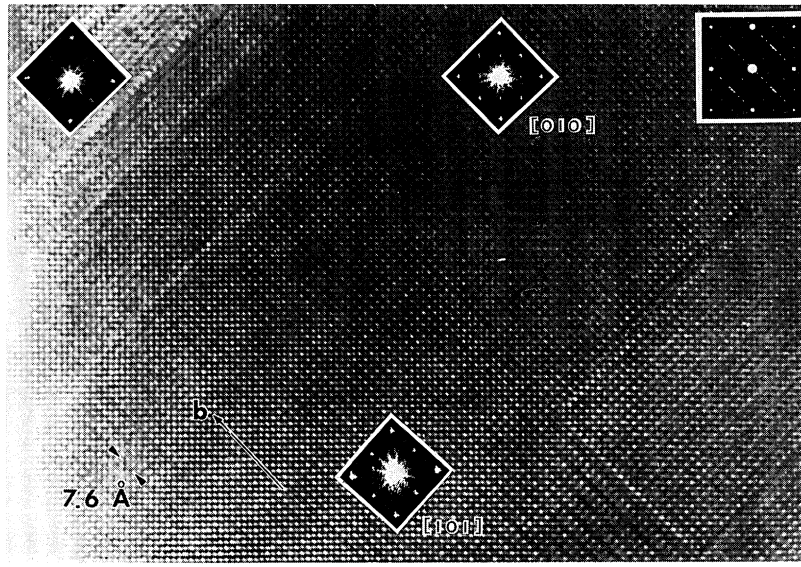

Figure 9. 90° rotation twinning in a predominantly $n = \infty$ crystal having both $(010)_{orth}$ and $(101)_{orth}$ as rocksalt-like composition planes. The twin domains give optical diffractograms consistent with [010] and [101] zones and may be used to reconstruct the major features of the SAD pattern.

chosen because it is assumed that the alkaline oxide layers are sufficiently separated to have no bearing on the oddness or evenness of the n-value.) The data were not treated in a rigorous statistical sense, as the sampling technique could not be random. The frequency histogram for orthorhombic material (figure 8*a*) shows that the $n = 3$ polytype is most common, with other n-members occurring much less frequently. By contrast, tetragonal structures exhibit a more even distribution in n-member frequencies (figure 8*b*), with a weak bimodal distribution peaking at $n = 3$ and 5. In agreement with observations for mineral systems in general (Price & Yeomans 1984), shorter stacking sequences are favoured over long period members. These data suggest that the oddness or evenness of stable members is dependent on symmetry, but largely independent of Ca/Sr stoichiometry (providing it is not so variable as to cause a change in symmetry).

(*c*) *Twin and domain structure*

Many preparations contained the orthorhombic perovskite parent structure, i.e. $Ca_xSr_{1-x}TiO_3$, $x < 0.25$. Such crystals usually exhibited 90 ° rotation twinning about the normals to the $\{101\}_{orth}$ and $(010)_{orth}$ planes, these being equivalent to $\langle 100 \rangle$ of the cubic subcell. It is noted that the composition planes of such twins are crystallographically quite complex, and, except in rare cases, not parallel to the twin rotation axis. Therefore, the atomic arrangement at the composition plane was not generally amenable to rigorous examination by HR imaging (White *et al.* 1985).

Rotation twinning also occurred in the layered structures, but in contrast to the aristotype, the composition planes were always well defined crystallographically, consisting of inserted CaO layers, and as such were suitable for direct interpretation by HREM. In the tetragonal, strontium-rich polytypes, oxide layers are inserted on the $\{100\}_{tet}$ planes. This behaviour persisted in the orthorhombic (pseudotetragonal) perovskites, as the $\{101\}_{orth} = \{100\}_{tet}$ and $(010)_{orth} = (001)_{tet}$ planes, which differ

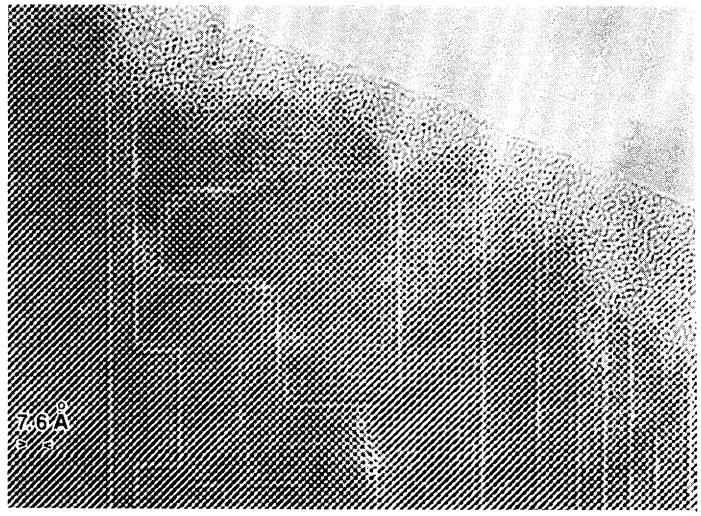

Figure 10. $[101]_{orth}$ projection of mosaic intergrowth area with CaO boundaries appearing on $(010)_{orth}$ and $(101)_{orth}$. ($\Delta f = -375$ Å.)

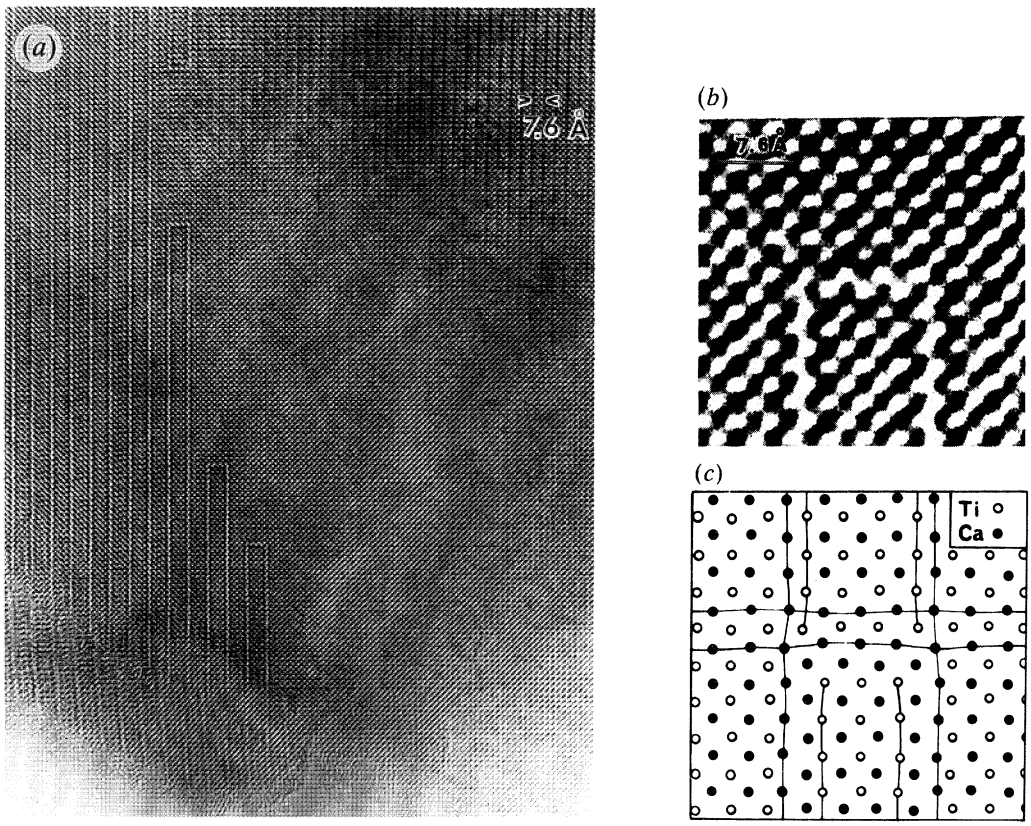

Figure 11. (*a*) Lower magnification $[101]_{orth}$ image of Ca-rich $n = 3$ structure intergrown with $CaTiO_3$. Note the four examples of bridging by CaO layers across the $n = 3$ polytype. (*b*) Enlargement of one bridge ($\Delta f = -375$ Å) and (*c*) schematic illustration of cation relaxation about the bridge taken directly from the HR image.

PHILOSOPHICAL TRANSACTIONS OF THE ROYAL SOCIETY A MATHEMATICAL, PHYSICAL & ENGINEERING SCIENCES

slightly in their TiO_6 tilt motifs, were all used to accommodate the excess alkaline earth oxide (figure 9). However, our observations show that rocksalt layers form more frequently on the $(010)_{orth}$, suggesting that these planes are energetically favoured over $\{101\}_{orth}$.

On occasion, the formation of oxide boundaries on the various pseudotetragonal planes occurred to a spectacular degree producing a mosaic of perovskite domains (figure 10). Such microdomains were usually adjacent to large areas (several hundred ångströms in extent) of the perovskite aristotype and serve as regions of stoichiometric transition between layered and unlayered perovskites. Small domain clusters within layered structures serve a similar function. Significantly, perovskite domains have never been observed to be completely bounded on all four edges by alkaline oxide layers, possibly as a result of lattice strain effects. Often, the oxide layers propagate by a series of right angled kinks to finally terminate in the aristotype (figure 10). Such terminations also occur in isolation within both ordered and disordered layer structures.

A model for the structure generated by simple rocksalt layer bridging across an $n = 3$ member was constructed directly from HR micrographs (figure 11). Atomic displacement contours show there is an outward relaxation at the termination of the $n = 3$ structure to accommodate the insertion of the oxide layer. There is also inward relaxation within the $n = 3$ domain. These displacement contours reflect the higher lattice free energy imposed by mosaics; by implication such mosaics are not equilibrium structures.

5. Discussion

(*a*) *Factors influencing the stability of n-members*

Because alkaline earth titanates are of technological importance as capacitors and positive temperature coefficient thermistors they have been the subject of extensive investigation, including structural characterization. In particular, when significant cation–cation non-stoichiometry is tolerated in a single phase system, the resulting changes in ionic defect concentrations can affect charge and mass transport and oxidation–reduction equilibria (Han *et al.* 1985). To better understand the anomalous electrical properties exhibited by some dielectrics, the conditions which favour the formation of point and extended defects require examination. To this end, two studies have recently appeared in which *ab initio* computational techniques were used to calculate the energies of formation for Ruddlesden–Popper type superlattices (Udayakumar & Cormack 1988, 1989). A summary of these results and some experimental observations are given in table 9.

Comparison of these data reveal considerable discrepancies between the calculated and experimental values of ΔH_f and also amongst the experimental datasets. For example, the measurements of Kubaschewski (1983) for Ca end-member phases show the $n = 3$ member ($\Delta H_f = +21$ kJ mol^{-1}) should be more stable than the $n = 2$ member ($\Delta H_f = +29$ kJ mol^{-1}), in agreement with our microscopic study where $n = 3$ was favoured over other members (see figure 8*a*). Udayakumar & Cormack (1989) also claim support for this conclusion from their theoretical treatment predicting $\Delta H_f = +18.0$ kJ mol^{-1} and $+17.4$ kJ mol^{-1} for $n = 2$ and $n = 3$ respectively. However, they also contend that the same positive ΔH_f value for the $n = 1$ member indicates that Ca_2TiO_4 itself will not be thermodynamically viable, but $CaTiO_3$ may incorporate individual Ruddlesden–Popper layers. Although this conclusion is in

Table 9. *Formation enthalpies of Ruddlesden–Popper compounds*

n-member	composition	ΔH_f[a] (kJ mol^{-1})	reference
3	$Ca_4Ti_3O_{10}$	+21	(*b*), (*e*)
		+17.4	(*c*)
	$Sr_4Ti_3O_{10}$	+25	(*b*), (*e*)
		−13.5	(*d*)
2	$Ca_3Ti_2O_7$	+29	(*b*), (*e*)
		+5.8	(*a*)
		+18.0	(*c*)
	$Sr_3Ti_2O_7$	−13.5	(*d*)
1	Ca_2TiO_4	+18.0	(*c*)
	Sr_2TiO_4	+46	(*b*), (*e*)
		−23	(*a*)
		−10.6	(*d*)

[a] $\Delta H_f = \Delta H_f(A_{n+1}Ti_nO_{3n+1}) - \Delta H_f(AO) - n\Delta H_f(ATiO_3)$.

(*a*) Wagman *et al.* (1982), (*b*) Kubaschewski (1983), (*c*) Udayakumar & Cormack (1989), (*d*) Udayakumar & Cormack (1988), (*e*) Weast (1978).

agreement with earlier X-ray investigations (Roth 1958) and the present study, it appears that the atomistic approach is not yet able to differentiate between the stability of calcium titanate perovskites. In particular, Udayakumar & Cormack (1989) found that ΔH_f values were insensitive to small changes in atomic coordinates which accompany the tetragonal–orthorhombic transition. In the case of Sr end members, they predict no thermodynamic differentiation beyond $n = 2$, whereas both microscopic and thermodynamic studies suggest that as n passes from 1 to 3 a minimum in ΔH_f occurs at $n = 2$.

This analysis shows that in the absence of reliable thermodynamic predictions, it would be valuable if some simple crystallochemical criterion could be devised to determine whether a Ruddlesden–Popper perovskite will form in a given chemical system. One possible approach, which has been used successfully in the case of ABX_3 perovskites, is to consider cation radius ratios to derive a tolerance factor (t) (Megaw 1973)

$$t = (r\mathrm{A} + r\mathrm{B})/\sqrt{2}(r\mathrm{B} + r\mathrm{X}).$$

Ruddlesden & Popper (1957) noted in the case of the $n = 2$ compounds Sr_2TiO_4, Ca_2TiO_4 and $SrLaAlO_4$ that $0.95 < t < 0.985$, and in those cases where $t < 0.95$, the K_2NiF_4 structure was destabilized. They suggest that the radius of the A ion cannot be reduced much below that satisfying the geometrical condition for close packing. Yokokawa *et al.* (1989) have argued that enthalpies of formation of K_2NiF_4-types can be well characterized in terms of t.

Poix (1980) developed a tolerance factor specifically for A_2BX_4 $n = 1$ layered perovskites which contain A cations in nine-fold coordination only. To derive this t factor a simplified tetragonal unit cell was assumed in which the nine A–X and six B–X bondlengths are respectively considered equal. These constraints are met when the separation of perovskite layers along c equals half the length of one octahedron. This does not closely approximate the real case even in the K_2NiF_4 structure type, where the separation across the rocksalt layer is 2.62 Å compared with the half-octahedral distance of 1.97 Å. Practically, the criteria of equal bondlengths is never

PHILOSOPHICAL TRANSACTIONS OF THE ROYAL SOCIETY A MATHEMATICAL, PHYSICAL & ENGINEERING SCIENCES

realized and the tolerance factors obtained by this method are a rough guide only. Given the limitations of this approach, Poix determined that A_2BX_4 structures will be stable when they satisfy the condition that $1.02 > t > 0.85$ in the formula:

$$t = \psi_A \sqrt{2}/2\beta_B,$$

where ψ_A and β_B are the average A–X and B–X bondlengths respectively. Formulae to calculate the average bond lengths are given in Poix (1980). (There is a typographical error in Table II of Poix (1980). The first equation should read $\psi_1 = c(z_1 - z_2)$ and its footnote should read $z_1 \sim 0.35$ and $z_2 \sim 0.15$.) However, many anomalies exist when one compares t-factors (calculated by idealizing atom positions and symmetry) with compilations of known compounds. For example, Poix comments that he cannot explain the non-existence of cadmium compounds with this structure type. Furthermore, and of particular relevance to this work, the t factor for Ca_2TiO_4 is calculated to be 0.98 suggesting that this compound may be stable, however, this phase has not been observed (at room temperature and pressure). (For this hypothetical phase the following data were assumed for the calculation of a t factor: a = the average of $a+b$ for $Ca_3Ti_2O_7$, $c = 2 \times$ octahedral height $+ 2 \times$ rocksalt thickness for $Ca_3Ti_2O_7$, $z_1 = 0.35$, $z_2 = 0.15$.) Therefore, it would appear that a geometrical method for predicting the existence of $n = 1$ compounds is inconclusive. Accordingly, it is unlikely that this approach would be any more successful for higher n-members.

(*b*) *Point and extended defect formation*

Frequently, information regarding point defect data is collected indirectly by equilibrium conductivity measurements (Han *et al.* 1985). However, these procedures have led to conflicting point defect models for perovskites of the same nominal composition (Udayakumar & Cormack 1989). Furthermore, in some instances the point defect model has been discarded in favour of Ruddlesden–Popper-like extended defects (Balachandran & Eror 1982; Choi & Tuller 1988).

It is generally believed that four point defect mechanisms operate to varying degrees. Excess AO may be incorporated by the generation of V''''_{Ti} and $V^{\cdot\cdot}_O$ as follows:

$$AO \longrightarrow A_A + O_O + V''''_{Ti} + 2V^{\cdot\cdot}_O. \quad (1)$$

Tentative support for mechanism (1) has come from HREM. An example of a column of Ti atoms in which the intensity is diminished with respect to surrounding columns is given in figure 12. A reasonable match with the experimental image was obtained by removing 25% of the Ti atoms. Since the surrounding atomic columns are of comparable intensity it may be inferred that charge compensation is achieved by the removal of nearby oxygens.

Alternatively, some A atoms may partition onto the Ti site:

$$2AO \longrightarrow A_A + A''_{Ti} + 2O_O + V^{\cdot\cdot}_O. \quad (2)$$

The electrical data of Han *et al.* (1985) imply that this mechanism is viable for both Ca and Sr titanate perovskites, but Udayakumar & Cormack's (1989) calculations suggest only Sr replacement for Ti is possible. However, from a purely crystal chemical viewpoint this conclusion seems unlikely, because the ionic radii of Ca and Ti are more closely matched to each other than to Sr. Furthermore, our neutron diffraction experiments did not indicate measurable partitioning of Sr or Ca onto Ti sites. It was not possible to distinguish cation $\leftrightarrow$ cation replacements by HREM as

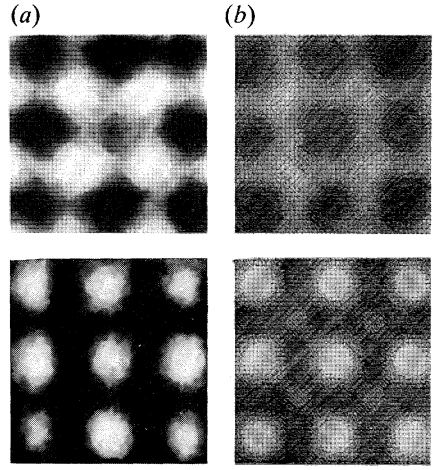

Figure 12. Experimental and simulated images of a 25% deficient Ti atom column in a crystal 21 Å thick. (*a*) $\Delta f = -375$ Å, (*b*) $\Delta f = -750$ Å.

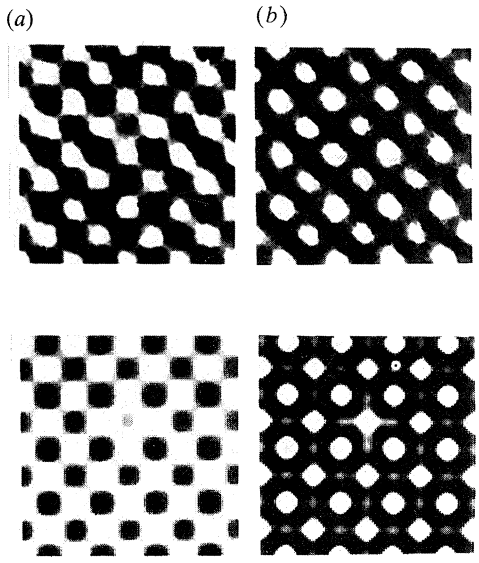

Figure 13. Experimental and simulated images of a 25% deficient Ca atom column in a crystal 18 Å thick. (*a*) $\Delta f = -375$ Å, (*b*) $\Delta f = -600$ Å.

image simulations confirmed that the scattering power of Ca, Sr and Ti were not sufficiently dissimilar to demonstrate site disorder amongst these species. Therefore, no information regarding the validity of mechanism (2) could be gleaned by this method.

The incorporation of excess Ti by replacement of A cations can be expressed by the following defect equation:

$$2TiO_2 \longrightarrow Ti_A^{\cdot\cdot} + Ti_{Ti} + 3O_O + O_I''. \tag{3}$$

This replacement is not considered likely because it involves insertion of an oxygen atom on an interstitial site. As explained above no data concerning this type of defect

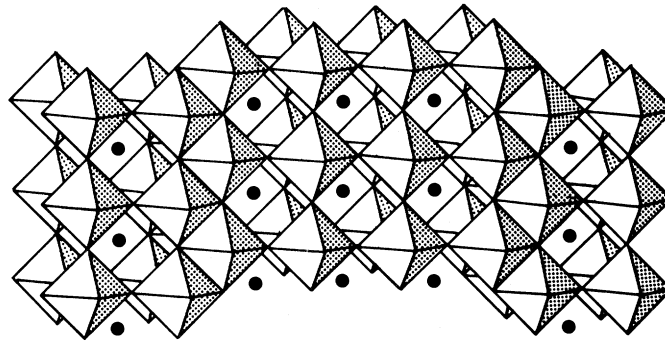

Figure 14. Perspective drawing of $6ABO_3 \cdot 2BO_2$.

could be derived from HREM, nor was it suggested by neutron diffraction. Alternatively, vacancies could be introduced on both the A and O sites.

$$TiO_2 \longrightarrow V''_A + Ti_{Ti} + 2O_O + V^{\cdot\cdot}_O. \quad (4)$$

Our HR micrographs indicate that this defect type may occur. Figure 13 shows an HR image of a crystal containing an alkaline earth deficient atomic column. A reasonable match using multislice calculations suggest a column occupancy of 75%.

Another method of incorporating excess TiO_2 is shown in figure 14. Here the perovskite blocks would shear not to produce AO layers but BO_2 extended defects; such intergrowths would form the basis of the $nABO_3 \cdot 2BO_2$ structural family. Defects of this sort have been seen by electron microscopy in the $KNbO_3$ and $NaNbO_3$ perovskites (Chen & Feng 1989), and would have been easily noticed by HREM if present in our titanate perovskites. None were observed, suggesting that only limited solubility of excess titanium is possible. This is in agreement with the scanning electron microscopy of Han *et al.* (1985) who found that rutile was invariably stabilized in $SrTiO_3$ having excess TiO_2 down to 0.5 mol% (Sr/Ti = 0.995).

In Ca rich and Sr rich perovskites with n nominally equal to infinity, isolated and clustered groupings of Ruddlesden–Popper structures could be located, particularly in samples that had been sintered for shorter periods. Although disordered insertion of rocksalt layers occurred in both the calcium and strontium end members, it seems likely that in mixed phases the diffusion of Ca plays a dominant role in promoting disordered intergrowths as this element, rather than Sr, partitions preferentially into the rocksalt layers. It is perhaps significant that the cation deficient columns recognized by HREM only occurred within finely textured mosaics (figure 10). Mosaics are believed to exist metastably during the transition from ordered to disordered structures (see §4*c*), and may provide Ca with a three-dimensional preferred diffusion path.

For our samples, no noticeable differences in the nature of extended defects between Ca rich and Sr rich phases could be found. This result is contrary to the conclusion of Udayakumar & Cormack (1989) whose calculations suggested that ordered insertion of Ruddlesden–Popper layers in Ca rich perovskite would be thermodynamically unstable. However, polysomatic disorder is undoubtedly linked to oxygen activity and no attempt was made in our experiments to control this parameter. Certainly, the conditions were not strongly reducing, as X-ray

PHILOSOPHICAL TRANSACTIONS OF THE ROYAL SOCIETY A MATHEMATICAL, PHYSICAL & ENGINEERING SCIENCES

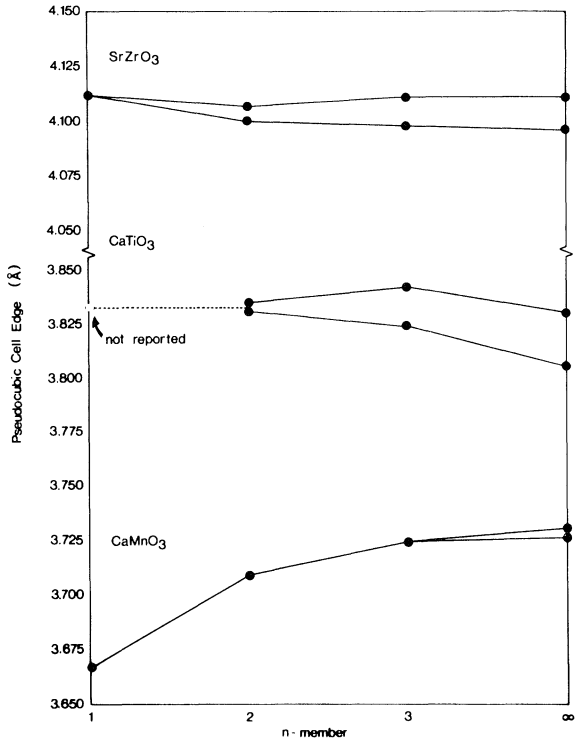

Figure 15. Trend from orthorhombic to tetragonal symmetry with decreasing n-value of (*a*) $SrZrO_3$, (*b*) $CaTiO_3$ and (*c*) $CaMnO_3$.

photoelectron spectroscopy did not indicate the presence of trivalent Ti (S. Myhra, personal communication). The imposition of lower oxygen activity, where oxygen vacancy formation could be favoured, may affect the extent of disorder.

(*c*) *Factors controlling the symmetry of Ruddlesden–Popper phases*

In general, only ABX_3 perovskites which exist in the cubic modification (at room temperature and pressure) will form $n = 1$ compounds (table 1). As only a remnant of the perovskite structure remains – a raft one BO_6 octahedron in extent – the energy to incorporate the cubic close packed AO rocksalt layer within a tilted BO_6 layer becomes excessive. When this rule is not adhered to, the departures from cubic symmetry are only slight. For $CaTiO_3$ the discrepancy between the pseudocubic axes is sufficient to destabilize the $n = 1$ member. However, greater departures from cubic symmetry can be accommodated in Ruddlesden–Popper phases with $n > 1$, as evidenced by the occurrence of $Ca_3Ti_2O_7$ and $Ca_4Ti_3O_{10}$. This is because unlike the $n = 1$ compound, adjacent octahedra within a perovskite block may tilt and distort cooperatively, as in the aristotype, to stabilize the CaO layers. The result of these topological distortions is a trend towards tetragonality for smaller n-values.

A useful progression, which illustrates the relation between aristotype and layer perovskite symmetry, is the series passing from distinctly orthorhombic $CaTiO_3$ to moderately distorted $SrZrO_3$ and finally slightly distorted $CaMnO_3$ (figure 15). The degree of deviation from cubic symmetry is given in table 1. Although the distortion of $CaTiO_3$ from cubic is sufficient to destabilize the $n = 1$ polytype, the $n = 2$ and

Table 10. *The extended Ruddlesden–Popper family of general formula* $mAX \cdot nABX_3$ *including selected ceramic superconductors*

(Adapted from Smyth (1988).)

compound	AX component	ABX_3 component	$m:n$	
$Sr_4Ti_3O_{10}$	SrO	$SrTiO_3$	1:3	perovskite
$Sr_3Ti_2O_7$	SrO	$SrTiO_3$	1:2	rich
Sr_2TiO_4	SrO	$SrTiO_3$	1:1	
$Tl_2Ba_2Ca_2Cu_3O_{10}$	$(Tl_2Ba)O_3$	$(Ba, Ca_2)Cu_3O_9$	3:3	
$YBa_2Cu_3O_7$	—	$(Y, Ba)_3Cu_3O_9$	0:1	
$Tl_2Ba_2CaCu_2O_8$	$(Tl_2Ba)O_3$	$(Ba, Ca)Cu_2O_6$	3:2	
	no compound yet prepared		2:1	rocksalt
$Tl_2Ba_2CuO_6$	$(Tl_2Ba)O_3$	$BaCuO_3$	3:1	rich

$n = 3$ members do occur, albeit with orthorhombic symmetry. The strontium zirconate aristotype, is less distorted and favours the formation of a tetragonal $n = 1$ member, but maintains orthorhombic symmetry in the $n = 2$ and 3 members. $CaMnO_3$ has a unit cell only slightly removed from cubic, and consequently the $n = 1$, 2, and 3 structures all adopt tetragonal symmetry.

Because the ABX_3 aristotype must closely approach cubic symmetry for an $n = 1$ member to form, new members of the series might be produced at high temperature and pressure. $CaTiO_3$ transforms from orthorhombic to tetragonal symmetry at 600 °C, and to the cubic form above 1200 °C (Kay 1951). The simultaneous application of pressure might result in the $n = 1$ structure. Conversely, upon cooling to 107 K $SrTiO_3$ adopts a tetragonal cell (Hutton & Nelmes 1981) so the symmetry of $Sr_3Ti_2O_7$ and $Sr_4Ti_3O_{10}$ may be lowered from tetragonal to orthorhombic. Such experiments have been applied to compounds of geological interest that model the crystal chemistry of mantle phases. Reid & Ringwood (1970) not only prepared the high pressure cubic perovskite $CaGeO_3$ (to mimic the behaviour of $CaSiO_3$) but also Ca_2GeO_4.

The Ruddlesden–Popper phases are possibly far more chemically diverse than the available data suggest. For example, the altervalent compounds $(Na, Y)_{n+1}Ti_nO_{3n+1}$ ($n = 2, 3$) have been reported (Goodenough *et al.* 1970), but details of this investigation are not published. It is feasible for many of the charge coupled substitutions observed in ABX_3 perovskites to operate in layer perovskites also. A related family of $(Nd, Ca)_nTi_nO_{3n+2}$ perovskite derivatives have been synthesized in which oxide layers are inserted on the {110} pseudocubic planes rather than {100} (Nanot *et al.* 1976). Potentially, many complex structures are possible by the combination of suitable A-site cations.

(*d*) *Relation to oxide superconductors*

The Ruddlesden–Popper phases have long been implicitly recognized as the structural progenitors of ceramic high-temperature superconductors, which are at present the subject of considerable research effort. The description of high-temperature superconductors in terms of an extended Ruddlesden–Popper series has recently been enunciated by Smyth (1989). In this description, all superconductors are described by the general formula $nABX_3 \cdot mAX$ in which the $m:n$ ratio is often greater than 1; in other words the rocksalt slabs are wider than the perovskite layers. A summary of this description, based on the work of Smyth is given in table 10. It

PHILOSOPHICAL TRANSACTIONS OF THE ROYAL SOCIETY A MATHEMATICAL, PHYSICAL & ENGINEERING SCIENCES

is now clear, that the prototypical Ruddlesden–Popper phases are a special case in which $m = 1$, n is variable and (near) integral oxygen stoichiometry maintained. Because the structure building principle for ceramic superconductors and Ruddlesden–Popper phases is equivalent, it is not surprising that many superconductors display intergrowth structures in which there is either variation in the width of the rocksalt layers, the perovskite type layers or both (see, for example, Davies & Tilley 1987) in a manner similar to those described in this work.

K. H. thanks Professor B. G. Hyde, Research School of Chemistry, Australian National University, for access to the JEM 200CX microscope. X-ray photoelectron spectroscopy studies were undertaken by Dr S. Myhra, Division of Science and Technology, Griffith University, Queensland, Australia.

References

Ahtee, A., Ahtee, M., Glazer, A. M. & Hewat, A. W. 1976 *Acta crystallogr.* B **32**, 3243–3246.

Balachandran, U. & Eror, N. G. 1982 *J. Mater. Sci.* **17**, 2133–2140.

Coughanour, L. W., Roth, R. S. & DeProsse, V. A. 1954 *J. Res. N.B.S.* **52**, 37–42.

Chen, J. & Feng, D. 1989 *Phys. Status Solidi* A **116**, 231–235.

Choi, M. & Tuller, H. L. 1988 *J. Am. Ceram. Soc.* **74**, 201–205.

Davies, A. H. & Tilley, R. J. D. 1987 *Nature* **326**, 859–861.

Drys, M. & Trzebiatowski, W. 1957 *Roczniki Chem.* **31**, 489–496. (Abstract cited.)

Durst, D., Grotenhuis, M. & Barkow, A. G. 1950 *J. Am. Ceram. Soc.* **33**, 133–139.

Elcombe, M. M., Kisi, E. H., Hawkins, K. D., White, T. J. & Goodman, P. 1991 *Acta crystallogr.* B. (In the press.)

Fischer-Cripps, A. 1987 *X-ray Analytical Software*, Fischer-Cripps Laboratories, Physics Department, University of Technology Sydney, Sydney, Australia.

Glaisher, R. W. 1985 Aspects of HREM of tetrahedral semiconductors. Ph.D. thesis, University of Melbourne, Melbourne, Australia.

Goodenough, J. B., Gräper, W., Holtzberg, F., Huber, D. L., Lefever, R. A., Longo, J. M., McGuire, T. R. & Methfessel, S. 1970 In *Landolt–Börnstein – numerical data and functional relationships in science and technology*, vol. 4, part a (ed. K.-H. Hellwege & A. M. Hellwege), pp. 126–314. Heidelberg: Springer-Verlag.

Han, Y. H., Harmer, M. P., Hu, Y. H. & Smyth, D. M. 1985 In *Transport in nonstoichiometric compounds* (ed. G. Simkovich & V. S. Stubican), pp. 73–85. New York: Plenum Press.

Hazen, R. M. & Finger, L. W. 1982 *Comparative crystal chemistry*, p. 231. New York: Wiley.

Hoverstreydt, E. R. 1983 *J. appl. crystallogr.* **16**, 651–653.

Hutchison, J. L., Anderson, J. S. & Rao, C. N. R. 1977 *Proc. R. Soc. Lond.* A **355**, 301–312.

Hutton, J. & Nelmes, R. J. 1981 *J. Phys.* C **14**, 1713–1736.

Kay, H. F. 1951 *Report on researches with ferroelectric materials*. The Electrical Research Association, Technical Report L/T257. The British & Allied Industries Research Association, Thorncroft Manor, Donking Road, Leatherhead, Surrey.

Kay, H. F. & Bailey, P. C. 1957 *Acta crystallogr.* **10**, 219–226.

Koopmans, H. J. A., van de Velde, G. M. H. & Gellings, P. J. 1983 *Acta crystallogr.* C **39**, 1323–1325.

Kubaschewski, O. 1983 In *Titanium: physico-chemical properties of its compounds and alloys*. Atomic Energy Review No. 9, pp. 3–74. Vienna: International Atomic Energy Agency.

Kwestroo, W. & Paping, H. A. M. 1959 *J. Am. Ceram. Soc.* **42**, 292–299.

Lukaszewicz, K. 1958 *Angew. Chem.* **70**, 320. (Abstract cited.)

Lukaszewicz, K. 1959 *Roczniki Chem.* **33**, 239–242. (Cited in *Structure Reports* **24**, 440–441 (1960).)

McQuarrie, M. 1955 *J. Am. Ceram. Soc.* **38**, 444–449.

Megaw, H. D. 1973 *Crystal structures: A working approach*. London: W. B. Saunders.

Nanot, M., Queryroux, F., Gilles, J.-C. & Chevalier, R. 1976 *Acta crystallogr.* B **32**, 1115–1120.

Nanot, M., Queryroux, F., Gilles, J.-C. & Portier, R. 1981 *J. Solid State Chem.* **38**, 74–81.

Poix, P. 1980 *J. Solid State Chem.* **31**, 95–102.

Poeppelmeier, K. R., Leonowicz, M. E., Scanlon, J. C., Longo, J. M. & Yelon, W. B. 1982 *J. Solid State Chem.* **45**, 71–79.

Price, G. D. & Yeomans, J. 1984 *Acta crystallogr.* B **40**, 448–454.

Reller, A., Thomas, J. M., Jefferson, D. A. & Uppal, M. K. 1984 *Proc. R. Soc. Lond.* A **394**, 223–241.

Reid, A. F. & Ringwood, A. E. 1970 *J. Solid State Chem.* **1**, 557–565.

Roth, R. S. 1958 *J. Res. N.B.S.* **61**, 437–440.

Ruddlesden, S. N. & Popper, P. 1957 *Acta crystallogr.* **10**, 538–539.

Ruddlesden, S. N. & Popper, P. 1958 *Acta crystallogr.* **11**, 54–55.

Sasaki, S., Prewitt, C. T., Bass, J. D. & Schulze, W. A. 1987 *Acta crystallogr.* C **43**, 1668–1674.

Shannon, R. D. 1976 *Acta crystallogr.* A **32**, 751–767.

Smyth, D. M. 1988 In *Ceramic superconductors II research update 1989* (ed. M. F. Yan), pp. 1–12. Westerville, Ohio: American Ceramic Society.

Swanson, D. K. & Peterson, R. C. 1980 *Can. Mineral.* **18**, 153–156.

Tilley, R. J. D. 1977 *J. Solid State Chem.* **21**, 293–301.

Tilloca, G. & Perez y Jorba, M. 1964 *Rev. Hautés Temper. Réfract.* **1**, 331–342.

Udayakumar, K. R. & Cormack, A. N. 1988 *J. Am. Ceram. Soc.* **71**, C-469–C-471.

Udayakumar, K. R. & Cormack, A. N. 1989 *J. Phys. Chem. Solids* **50**, 55–60.

Vallet-Regi, M., Gonzalez-Calbert, J., Alario-Franco, M. A., Grenier, J. C. & Hagenmuller, P. 1984 *J. Solid State Chem.* **55**, 251–261.

Wagman, D. D., Evans, W. H., Parker, V. B., Schumm, R. H., Halow, I., Bailey, S. M., Churney, K. L. & Nuttal, R. L. 1982 *J. Phys. Chem. Ref. Data* **11**, *Suppl. 2*, 275–281.

Weast, R. C. (ed.) 1978 *CRC handbook of chemistry and physics*, pp. D64–D66. West Palm Beach, Florida: Chemical Rubber Publishing Company.

White, T. J., Segall, R. L., Barry, J. C. & Hutchison, J. L. 1985 *Acta crystallogr.* B **41**, 93–98.

Yokokawa, H., Kawada, T. & Dokiya, M. 1989 *J. Am. Ceram. Soc.* **72**, 152–153.

Received 9 January 1991; accepted 12 March 1991

PHILOSOPHICAL TRANSACTIONS OF THE ROYAL SOCIETY A MATHEMATICAL, PHYSICAL & ENGINEERING SCIENCES

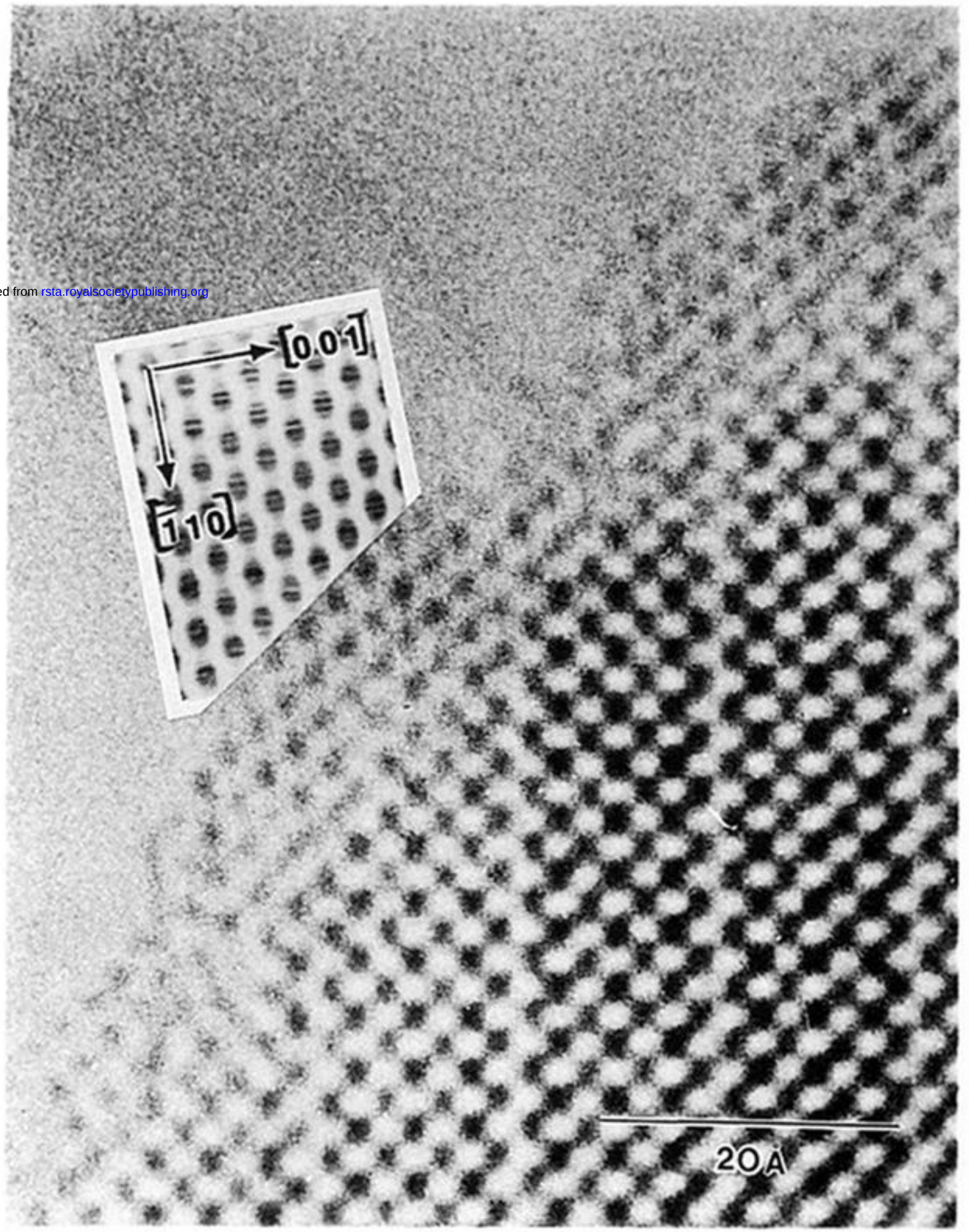

Figure 2. [110] TiO_x surface layer arising from electron beam-induced reduction of $3CaTiO_3 \cdot CaO$. (Calculation parameters: $T = 18$ Å; $\Delta f = -375$ Å.)

PHILOSOPHICAL TRANSACTIONS OF THE ROYAL SOCIETY A MATHEMATICAL, PHYSICAL & ENGINEERING SCIENCES

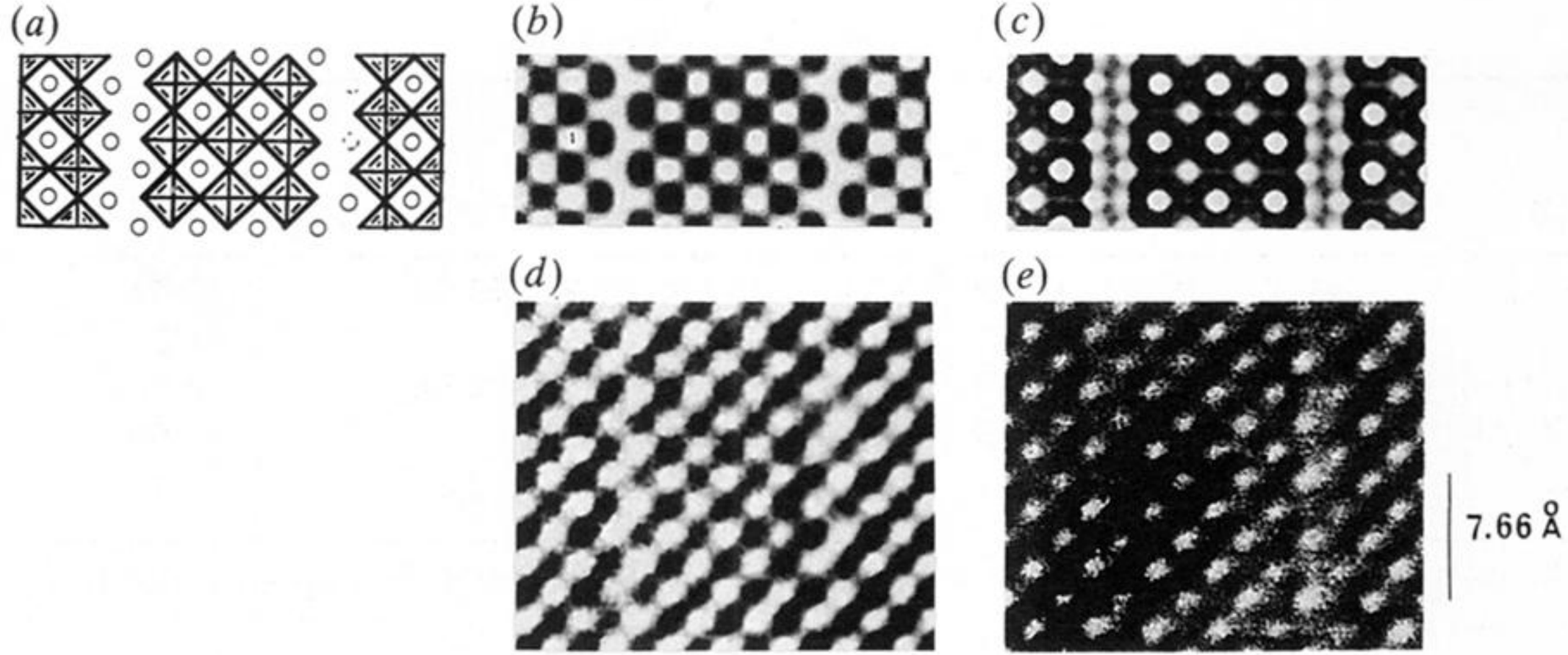

Figure 5. $[101]_{orth}$ schematic drawing (a) together with the simulated (b, c) and experimental (d, e) images from $Ca_4Ti_3O_{10}$. (Calculation parameters: $T = 24$ Å; $\Delta f = -375$ Å, -600 Å.) This image and subsequent high-resolution micrographs were collected using the JEM 4000EX microscope.

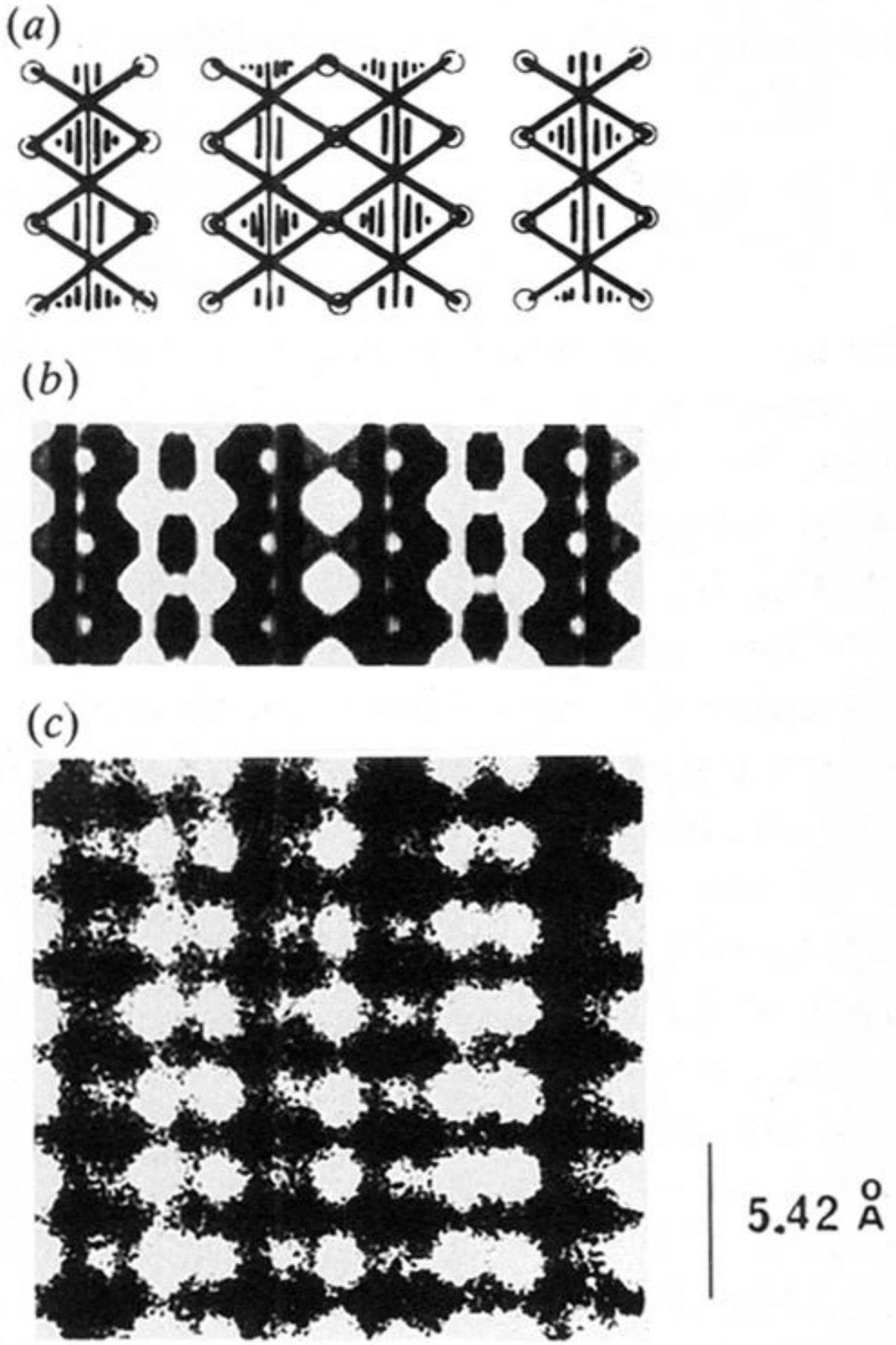

igure 6. $[100]_{orth}$ schematic drawing (a) together with the simulated (b) and experimental (c) images from $Ca_3Ti_2O_7$. (Calculation parameters: $T = 50$ Å; $\Delta f = -625$ Å.)

PHILOSOPHICAL TRANSACTIONS OF THE ROYAL SOCIETY A MATHEMATICAL, PHYSICAL & ENGINEERING SCIENCES

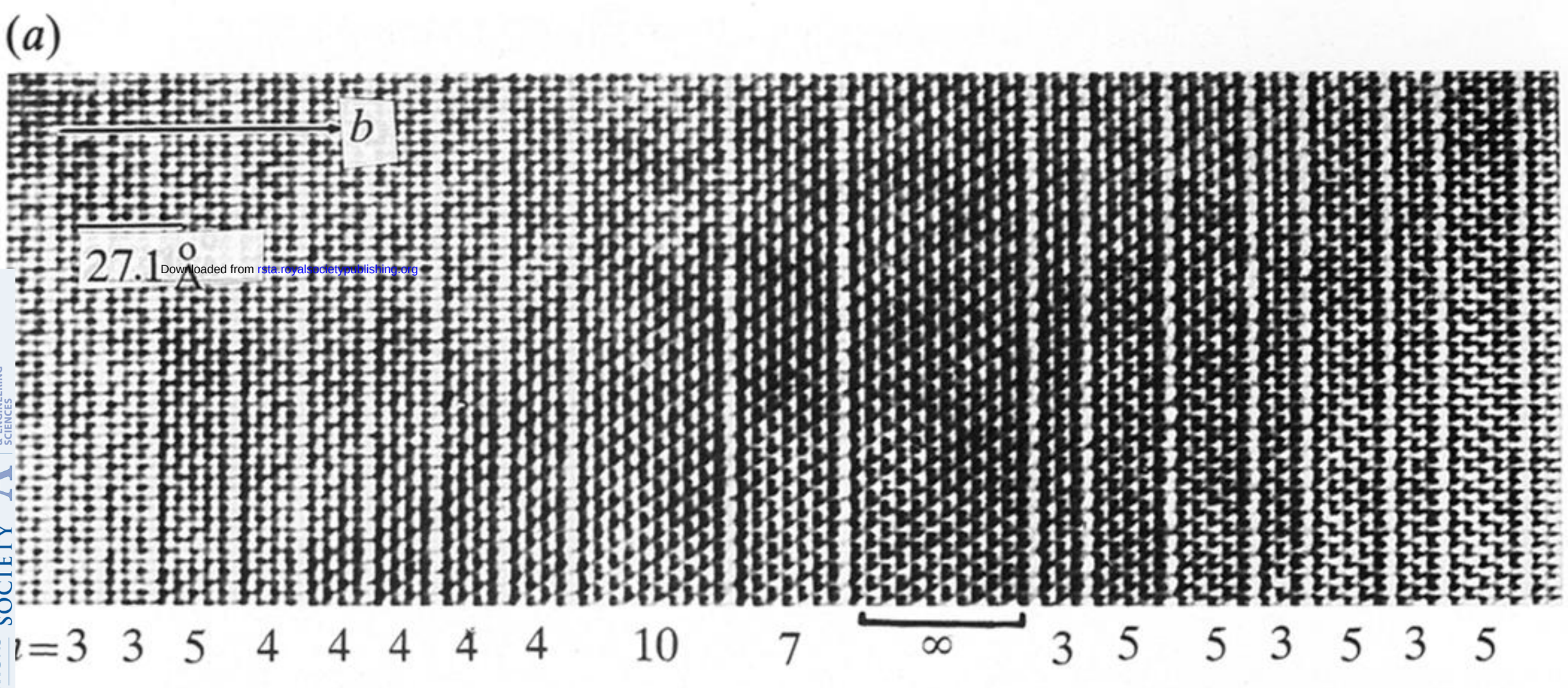

Figure 7. (*a*) $[100]_{orth}$ disordered intergrowth of polysomatic members. The fragment was from a compound of bulk stoichiometry of $Ca_4Ti_3O_{10}$ ($n = 3$) but represents a local average stoichiometry of $Ca_{5.53}Ti_{4.53}O_{14.69}$ ($n = 4.53$). The n-values were confirmed by optical diffractometry (*b–d*) which are components of the SAD pattern (*e*).

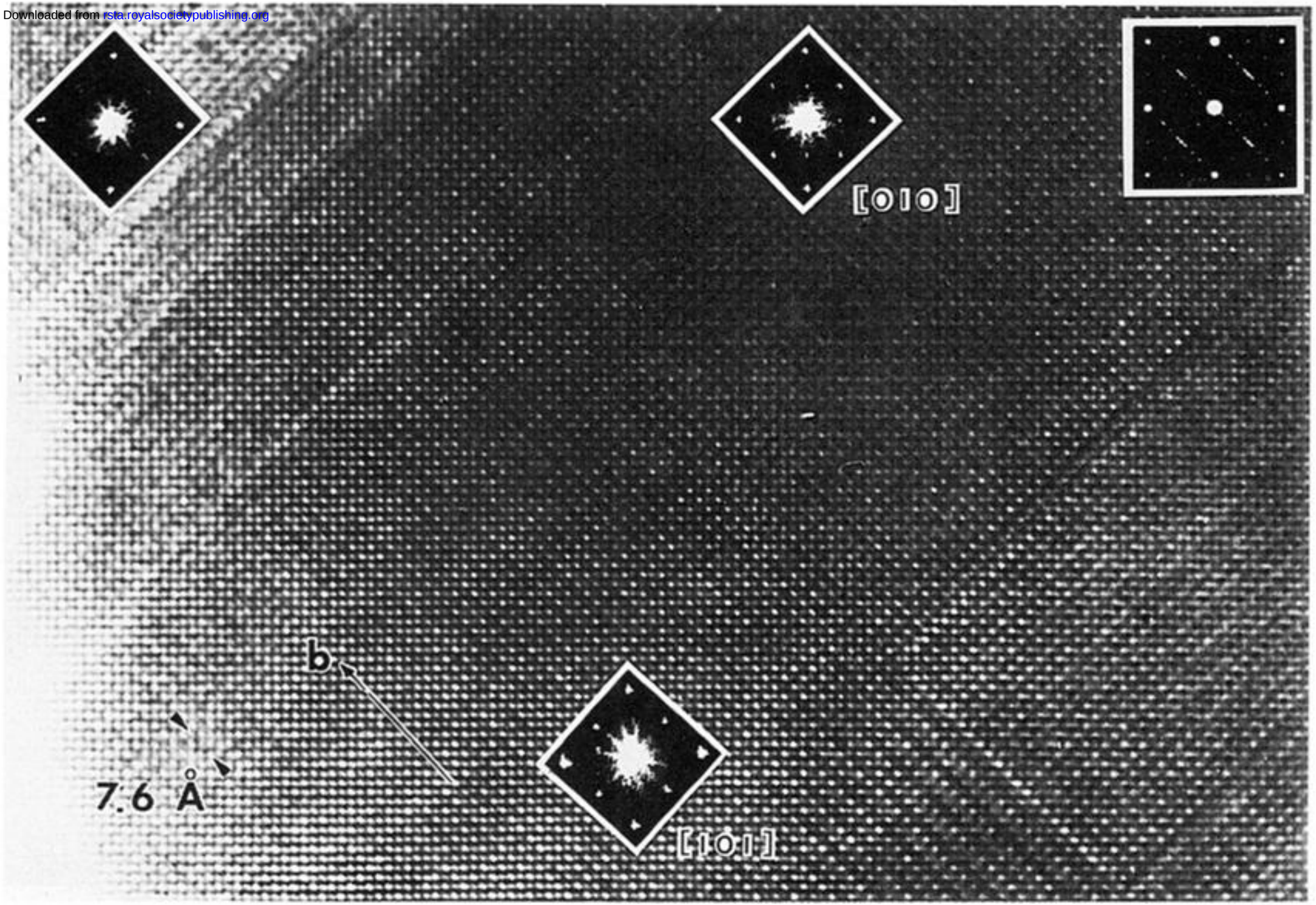

igure 9. 90° rotation twinning in a predominantly $n = \infty$ crystal having both $(010)_{orth}$ and $(101)_{orth}$ rocksalt-like composition planes. The twin domains give optical diffractograms consistent with 010] and [101] zones and may be used to reconstruct the major features of the SAD pattern.

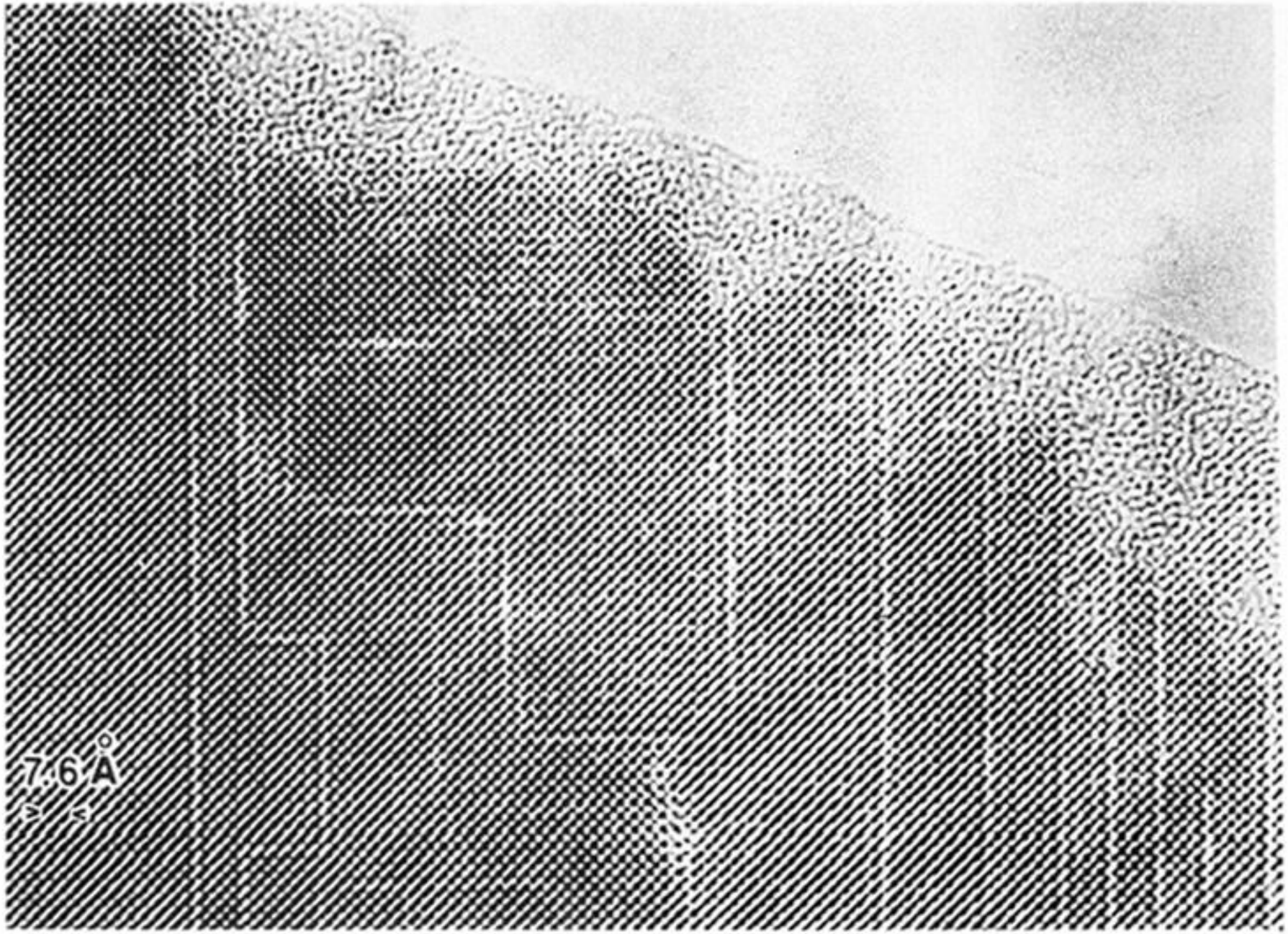

PHILOSOPHICAL TRANSACTIONS OF THE ROYAL SOCIETY A MATHEMATICAL, PHYSICAL & ENGINEERING SCIENCES

Figure 10. $[101]_{\text{orth}}$ projection of mosaic intergrowth area with CaO boundaries appearing on $(010)_{\text{orth}}$ and $(101)_{\text{orth}}$. ($\Delta f = -375$ Å.)

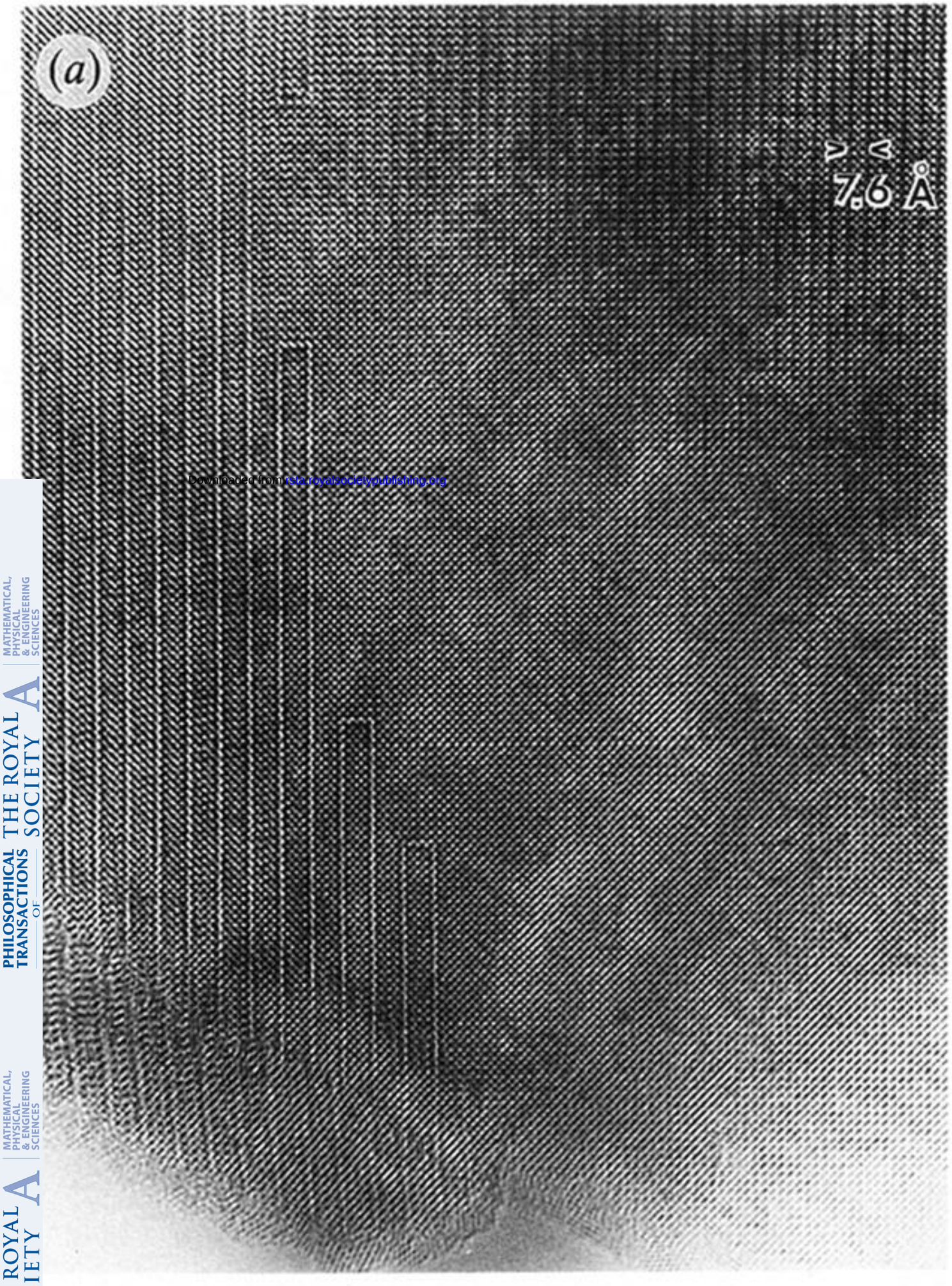

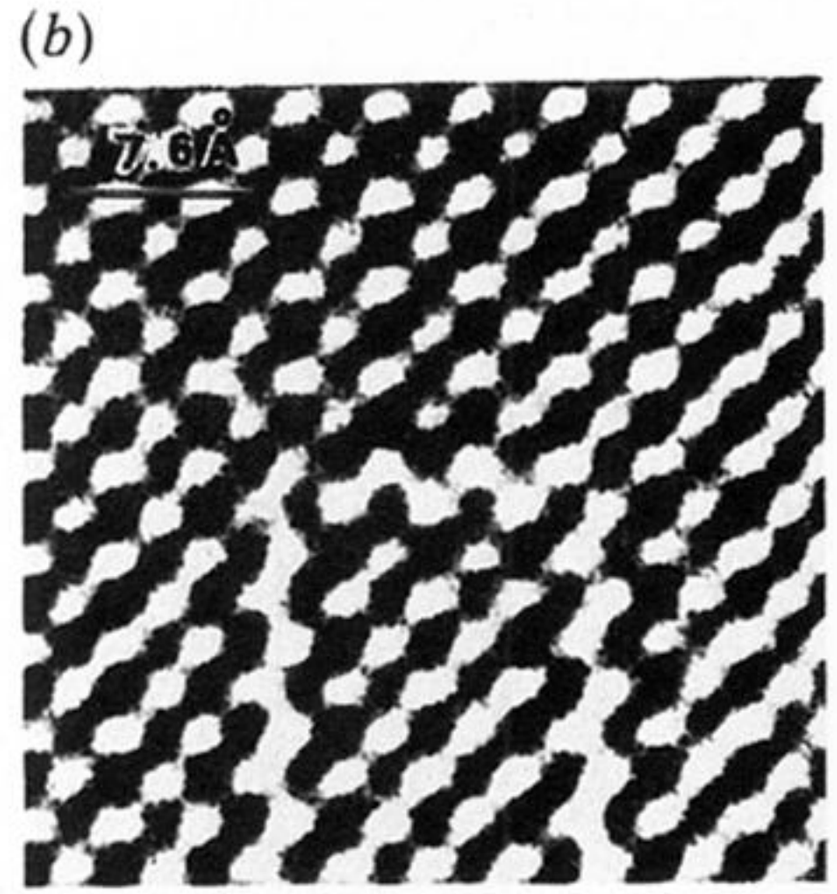

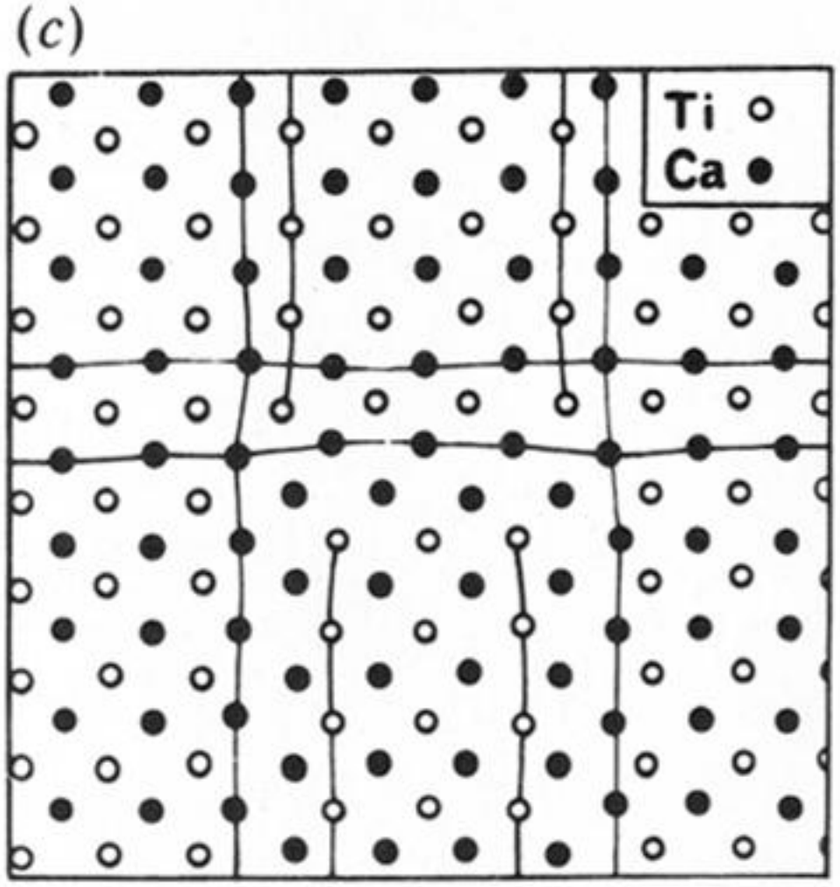

Figure 11. (*a*) Lower magnification $[101]_{orth}$ image of Ca-rich $n = 3$ structure intergrown with $CaTiO_3$. Note the four examples of bridging by CaO layers across the $n = 3$ polytype. (*b*) Enlargement of one bridge ($\Delta f = -375$ Å) and (*c*) schematic illustration of cation relaxation about the bridge taken directly from the HR image.

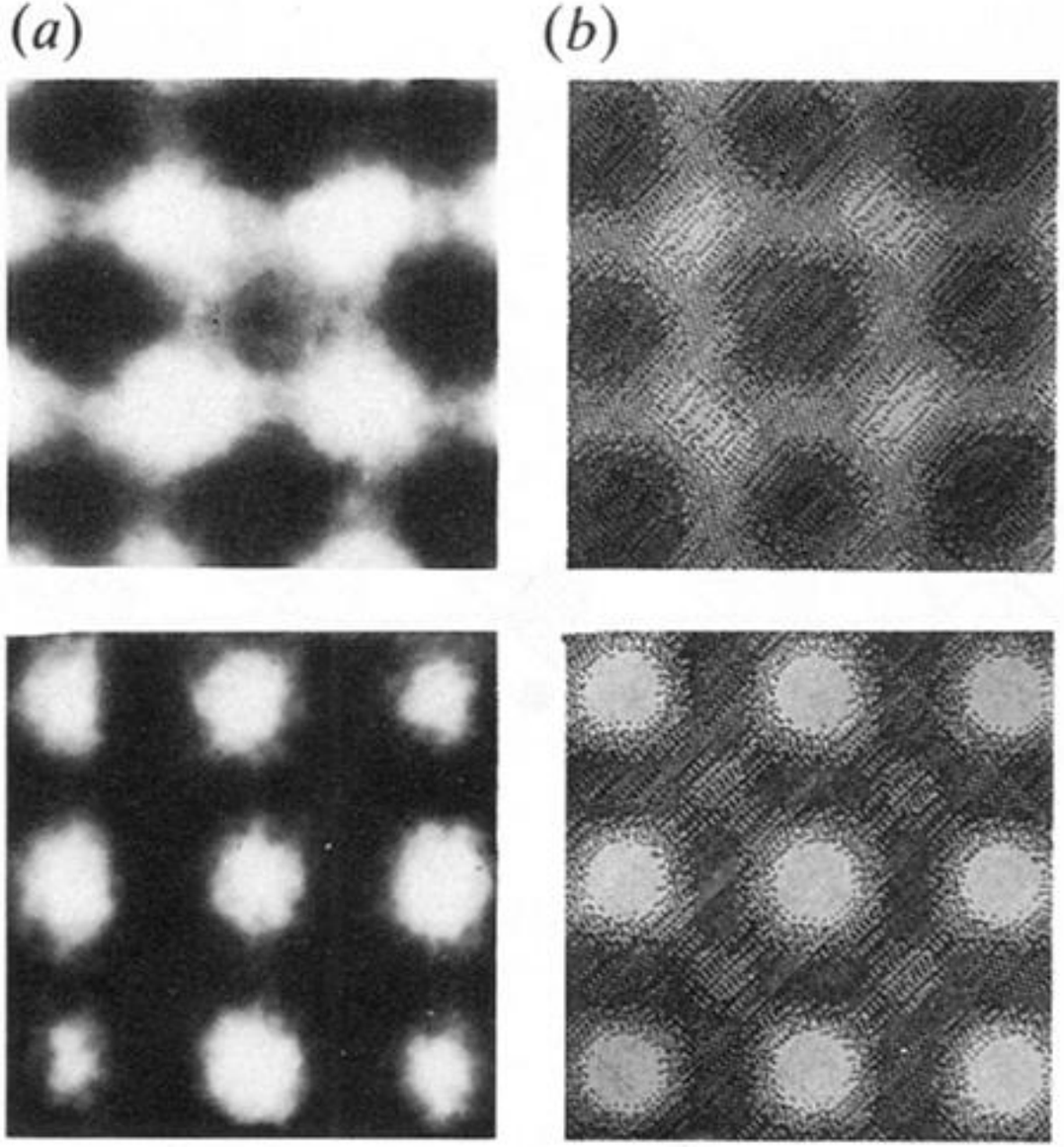

igure 12. Experimental and simulated images of a 25 % deficient Ti atom column in a crystal 21 Å thick. (*a*) $\Delta f = -375$ Å, (*b*) $\Delta f = -750$ Å.

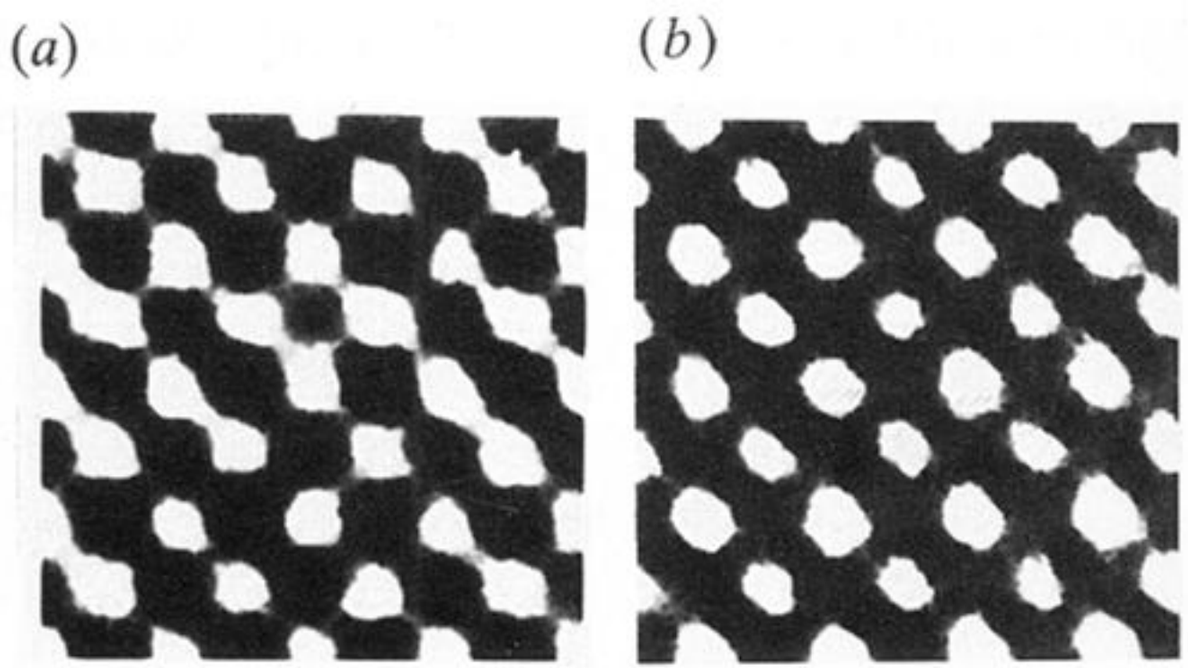

PHILOSOPHICAL TRANSACTIONS OF THE ROYAL SOCIETY A MATHEMATICAL, PHYSICAL & ENGINEERING SCIENCES

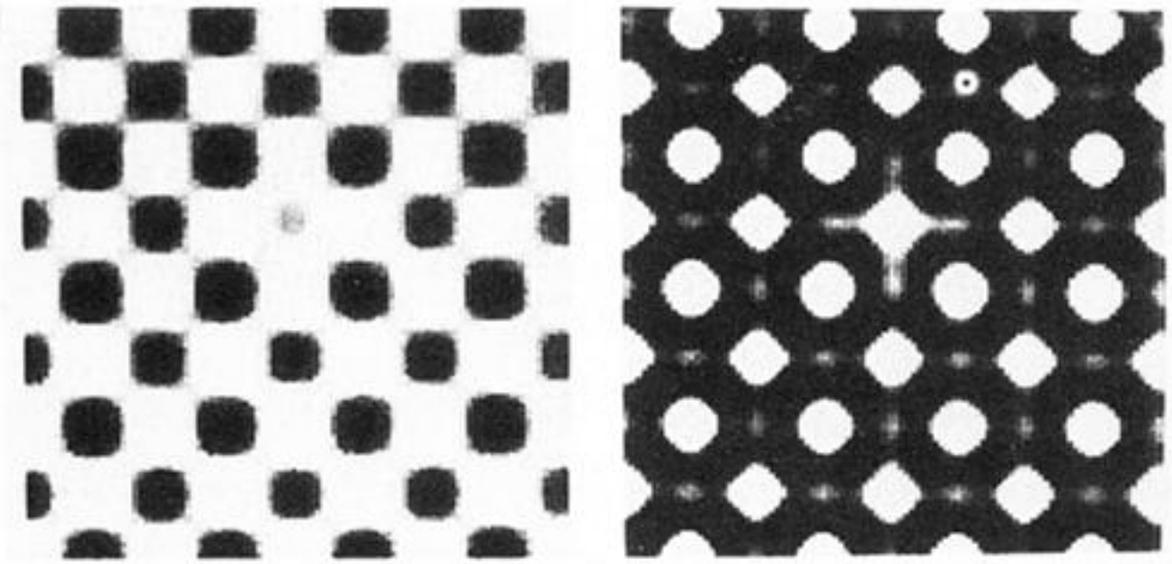

igure 13. Experimental and simulated images of a 25% deficient Ca atom column in a crystal 18 Å thick. (*a*) $\Delta f = -375$ Å, (*b*) $\Delta f = -600$ Å.